Forschungszentrum Karlsruhe
in der Helmholtz-Gemeinschaft

Wissenschaftliche Berichte
FZKA 6925

Actinide Migration Experiment in the ÄSPÖ HRL in Sweden: Results from Core #5 (Part III)

B. Kienzler, P. Vejmelka, J. Römer, D. Schild, F. Enzmann,E. Soballa, M. Fuß, F. Geyer, T. Kisely, A. Görtzen

Institut für Nukleare Entsorgung

Dezember 2003

Forschungszentrum Karlsruhe

in der Helmholtz-Gemeinschaft

Wissenschaftliche Berichte

FZKA 6925

Actinide Migration Experiment in the ÄSPÖ HRL in Sweden: Results from Core #5 (Part III)

B. Kienzler, P. Vejmelka, J. Römer, D. Schild, F. Enzmann*
E. Soballa, M. Fuß, F. Geyer, T. Kisely, A. Görtzen

Institut für Nukleare Entsorgung

*Johannes Gutenberg-Universität Mainz
Institut für Geowissenschaften
D-55099 Mainz

Forschungszentrum Karlsruhe GmbH, Karlsruhe

2003

Impressum der Print-Ausgabe:

Als Manuskript gedruckt

Forschungszentrum Karlsruhe GmbH
Postfach 3640, 76021 Karlsruhe

Mitglied der Hermann von Helmholtz-Gemeinschaft
Deutscher Forschungszentren (HGF)

ISSN 0947-8620

Abstract

Within the scope of a bilateral cooperation a series of **Actinide Migration Experiment** were performed by INE at the Äspö Hard Rock Laboratory in Sweden. This report covers investigations on actinide migration in a single fractured granite sample (core #5) performed in the CHEMLAB 2 probe under in situ conditions at Äspö HRL. The same experimental setup was applied as in previous experiments. Investigations of the flow path properties and the breakthrough of inert HTO tracer are reported. Experiments with the actinides Am, Np and Pu are presented. Breakthrough of actinides was not detected within the experimental time of about four months. The different analytical techniques for determination of sorbed actinides are presented. After cutting the core in slices, the abraded material is dissolved and analyzed, the slices are used to visualize the flow path. Effective volumes and inner surface areas are measured and the results compared to batch soption studies. A prediction for the breakthrough of a further in-situ experiment is given planned for uranium as tracer.

Actiniden Migration Experiment im Untertagelabor ÄSPÖ in Schweden: Ergebnisse zu Core #5 (Teil III)

Zusammenfassung

Im Rahmen einer bilateralen Zusammenarbeit wurde vom INE eine Reihe von Actiniden-Migrations-Experimenten im Hard Rock Laboratory Äspö in Schweden durchgeführt. Im vorliegenden Bericht sind Untersuchungen zur Actinidenmigration in einer einfach geklüfteten Granitprobe (Core #5) unter in-situ Bedingungen in der CHEMLAB-2 Sonde vorgestellt. Die Auslegung der Experimente erfolgte wie in den vorhergehenden Berichten beschrieben. Die Untersuchungen erstreckten sich über den Durchbruch eines inerten Tracers (HTO) und die Ermittlung der Fließweg-Parameter. Die Actiniden Am, Np und Pu wurden untersucht. Ein Durchbruch der Actiniden konnte innerhalb des experimentellen Zeitraums von 4 Monaten nicht beobachtet werden. Mit verschiedenen analytischen Methoden wurden die sorbierten Actiniden erfasst. Nach dem Zerschneiden des Bohrkerns wird das dabei abgeschliffene Material aufgelöst und analysiert, die Schnitte werden bezüglich des Fließweges visualisiert. Die effektiven Volumina der Kluft und ihre inneren Oberflächen werden bestimmt und die Ergebnisse mit Batch-Sorptions-Messungen verglichen. Die Ergebnisse werden für die Prognose des Migrationsverhaltens von Uran benutzt, das in einem weiteren Experiment eingesetzt werden soll.

CONTENTS

LIST OF TABLES

LIST OF FIGURES

1 Background and Objectives

The Äspö Hard Rock Laboratory (HRL) was established in Sweden in a granite rock formation for in-situ testing of disposal techniques and for investigations concerning migration and retention of radionuclides[Bäc91]. Groundwater flow through fractures in granite host rocks may cause migration of radionuclides from the repository. Within the scope of a bilateral cooperation between Svensk Kärnbränslehantering AB (SKB) and Forschungszentrum Karlsruhe, Institut für Nukleare Entsorgung (FZK-INE), actinide migration experiments with Pu, Am, and Np are conducted at the Äspö Hard Rock Laboratory.

The objectives of the in-situ actinide migration experiment in the Äspö HRL are directed to examine the applicability of laboratory data to natural conditions and to verify the laboratory sorption studies. The experiments aim to the reduction of uncertainties connected with the actinide behavior in a granitic environment. First sorption experiments are performed onto granite and "fracture filling material" in laboratory, then migration experiments in individual fractures in drill cores are performed in laboratory and in the Äspö HRL. To guarantee most realistic conditions - as close to nature as possible - the experiments are performed in the CHEMLAB 2 probe [Jan98]. An important aspect is the quantification of sorbed actinides after termination of the migration experiments. Therefore new methods had to be developed.

Previous reports summarize the results of batch experiments and migration experiments with core #1 and core # 4 in laboratory as well as results of the first in-situ experiment ([Vej2000], [Vej2001], [Röm2002], [Kie2002], [Kie2002a], [Kie2003], [Kie2003a]).

2 Materials

2.1 Groundwater

For laboratory investigations, Äspö groundwater was used, which was extracted from the drill hole SA 2600, whereas in the in-situ experiment natural groundwater is present in the CHEMLAB 2 borehole KJ0044F01. Both compositions are given in Ref. [Kie2003]. Both waters differ in the measured element concentrations by about 30-60%. Fe could not be measured in the groundwater used in laboratory (SA 2600). Fe had been precipitated during the transport to Germany.

The laboratory experiments were performed in a glove box at a 99% Ar, 1% CO_2 atmosphere. At Äspö HRL under the conditions prevailing in the CHEMLAB drill hole, the CO_2 partial pressure was computed to be log p_{CO2} = -2.6 which was only slightly different as in laboratory glove box (log p_{CO2} = -2.0).

2.2 Solid materials

A substantial prerequisite for the experiments was to get suitable drill cores containing single well characterized fractures. The cores #5, #6, and #7 were excavated from drill hole KOV 01 778.50-779.25. Transmissive and reflective light microscopy and Secondary Electron Microscopy (SEM) carried out at Geovetarcantrum, Göteborg University. The fracture is described by Ref. [Tul2002]: “The fracture is a vertical/subvertical fracture at ca 770 metres depth in the vertical borehole KOV 01 in Oskarshamn. The fracture is situated in a contact zone between fine-grained aplitic granite and a granitoid of Ävrö granite type. The wall rock on both sides is heavily tectonised and altered/oxidised. The breakdown of biotite is complete and has resulted in formation of chlorite. The plagioclase is saussuritisised. The fracture is several mm wide with different layers of K-feldspar, epidote/chlorite, (Fe(III) oxide/hydroxide) and calcite. The outermost layer is K-feldspar and epidote. Small grains of calcite and sericite are also present. The alteration has caused voids coated with K-feldspar crystals and these pores/voids are partly connected with the major fracture by micro fractures. The active surface may therefore be much enlarged along this fracture plane. Most of the surfaces seem to be covered with hydrothermally grown K-feldspar crystals (Adularia) or epidote but redistribution of quartz is also associated with the hydrothermal alteration and it is possible that other parts of the fractures are coated with hydrothermally grown quartz crystals. Micrograins of Fe(III) oxides are mostly associated with the epidote. The fracture present in the studied part of the drill core is part of a prominent hydrothermally altered fracture zone, which can be compared with the larger fracture zones at Äspö.”

Granite and "fracture filling material" of the drill cores were also analyzed regarding elemental composition and mineralogical phases by FZK-INE. The material covering the fracture surfaces was analyzed by scanning electron microscopy (SEM). Results of element mapping of granite and the altered material in a fracture are shown in Fig. 2-2. In unaltered granite, SiO_2 dominates, whereas in the altered material other main phases containing Al, K, Mg and Ca are present. Iron oxide containing particles showed Fe-concentrations by a factor of 200 above concentrations in the surrounding rock. X-ray diffraction pattern showed the mineral chlorite as a main constituent [Röm2002]. These findings agree well with those of SKB (Terralogica AB).

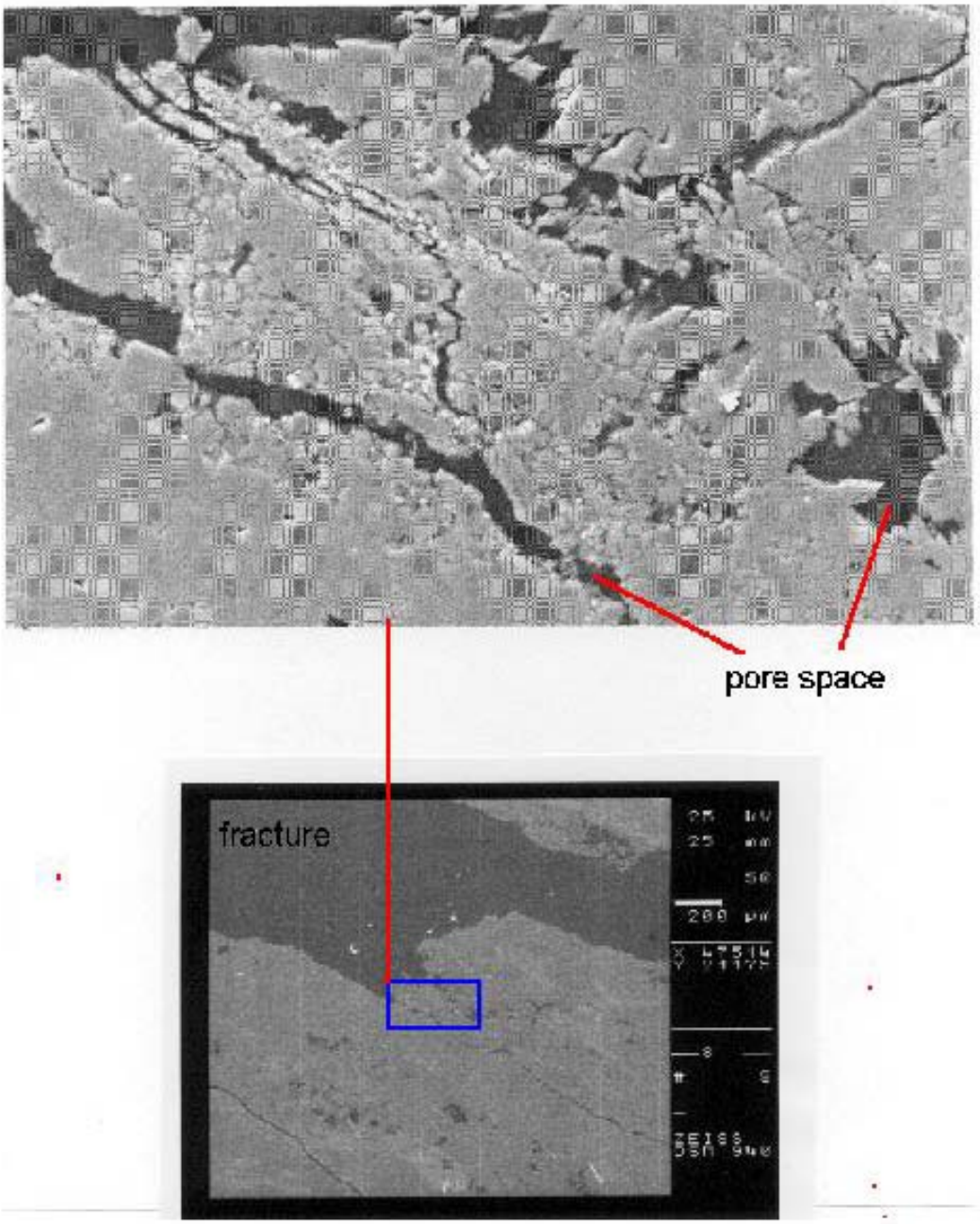

Fig. 2-1 Voids caused by alteration of granite coated with K-feldspar crystals partly connected with the major fracture by micro fractures.

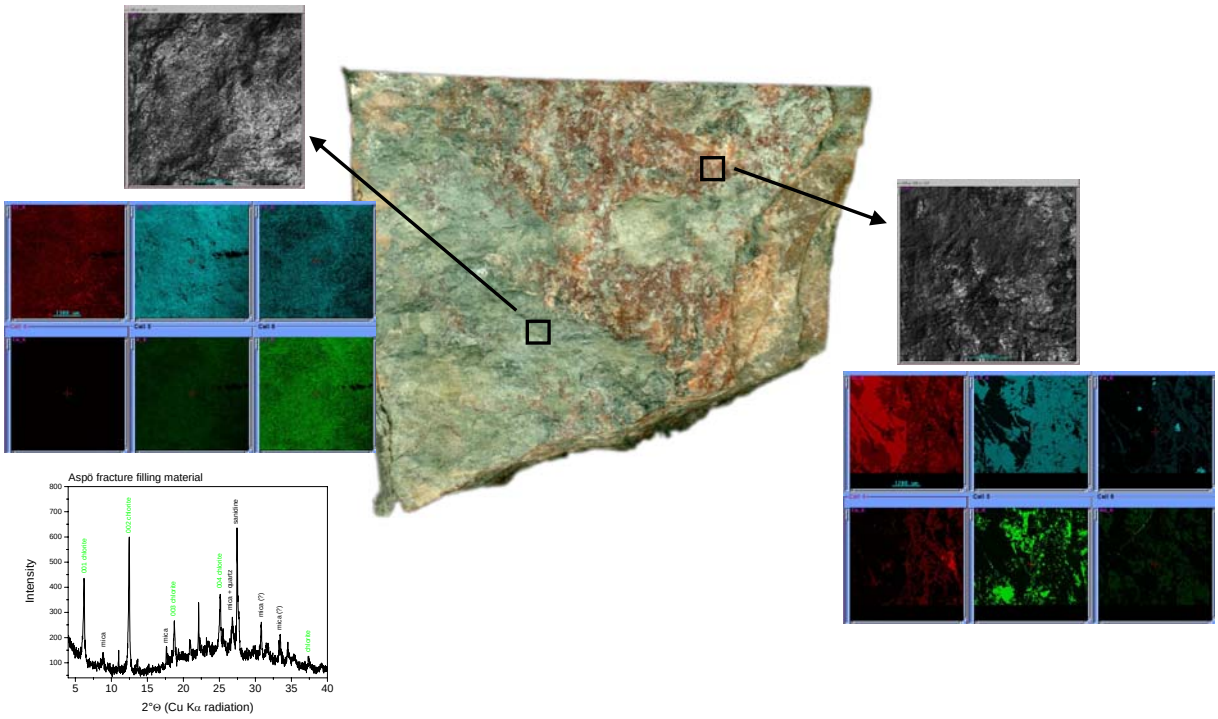

Fig. 2-2 Results of scanning electron microscopy (EDX-SEM) analysis of the fracture from drill hole KOV 01 778.50-779.25

Element mapping images and diffraction pattern of altered material (left) and of granite (right)
up: Si, Al, Fe, below: Ca, K, Na

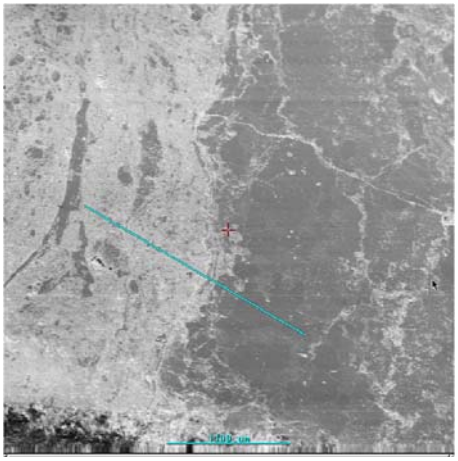

Fig. 2-3 Line indicating elemental line scan in samples from drill hole KOV 01 778.50-779.25

By EDX-SEM line scan analysis, the element concentration along a line from altered rock into the granite could be determined. This line (Fig. 2-3) had a length of 2.5 mm. The light part in the figure corresponds to altered material, the darker part to unaltered granite.

The element composition determined along the line is given in Fig. 2-4. It is obvious from Fig. 2-4 that Si dominates in the unaltered material (right). Probably, the elemental line scan hits a quartz grain. The altered material is characterized by a much broader distribution of elements, such as Al, Ca, Mg, and K. Si concentration scatters around 40%. Significant positive correlation between Si and K concentrations could be computed for the altered material, negative correlations between Si and Ca concentrations.

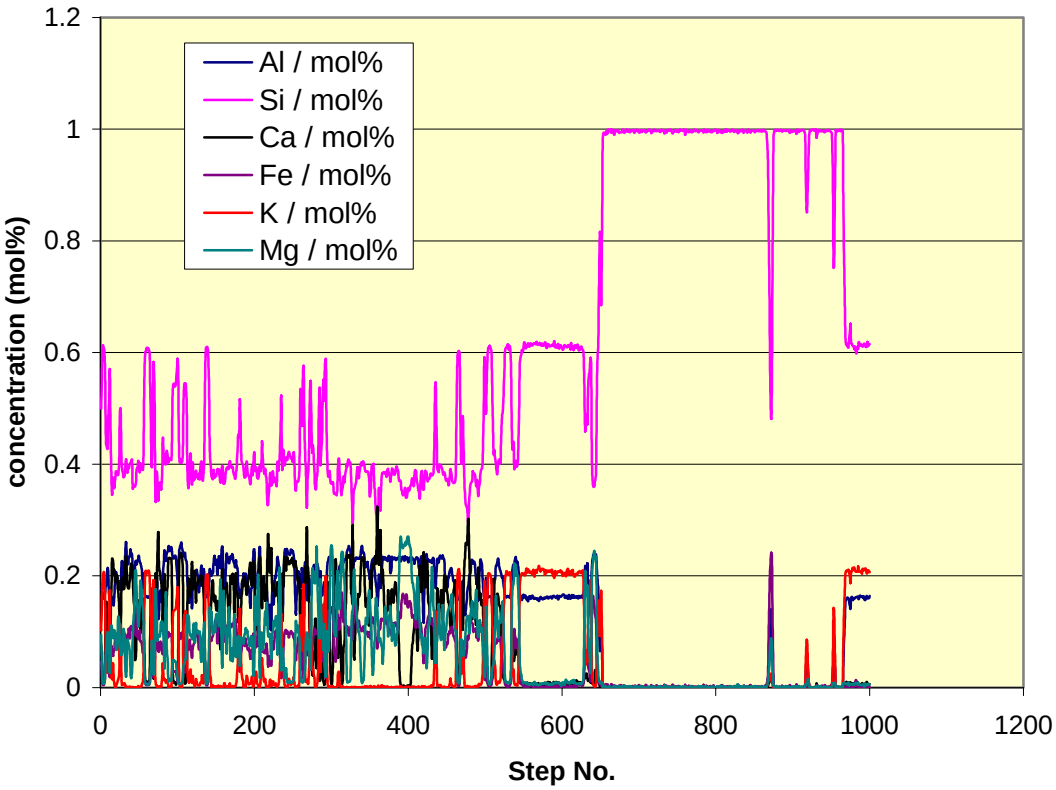

Fig. 2-4 Element distribution along a line from altered to unaltered material in KOV 01 778.50-779.25

1000 steps of line scan for 2.5 mm
0 < n < 645: altered material; n ≥ 645: unaltered granite

2.3 Sorption behavior of the solids

In order to evaluate the effect of specific minerals on the sorption behavior of the rock samples, a selection of minerals including those typical for granite were investigated [Kie2003a]. The minerals include: biotite, chlorite, muscovite, albite, orthoclase, apatite, epidote, titanite, zeolites, Mn- and Fe-oxides. For batch experiments, actinide spiked groundwater SA 2600 was prepared using the actinides ^{238}Pu, ^{237}Np and ^{233}U. Concentrations applied were 1×10^{-9} mol dm^{-3} (7.5×10^{5} Bq dm^{-3}) for ^{238}Pu, 1×10^{-4} mol dm^{-3} (5×10^{5} Bq dm^{-3}) for ^{237}Np and 1×10^{-5} mol dm^{-3} (8.4×10^{5} Bq dm^{-3}) for ^{233}U. The pH measured in the different spike solutions was 6.9 to 7.1.

Sorption experiments were performed with granite and fracture filling material. Strong sorption was observed for all actinides. Am and Pu showed marked sorption already after a very short contact time (1 - 2 days). Significant sorption was observed for Np in the presence of fracture filling material, where a redox potential of +50 mV was measured, only after 18 days.

While the Np concentration in the stock solution remained constant over the entire test period of 3 months, a continuous decrease was observed in the presence of fracture filling material. According to existing thermodynamic data, a reduction of Np(V) to the tetravalent state can be expected at redox potentials below +100 mV. This indicates clearly that reduction of Np(V) precedes the sorption reaction. A slow sorption kinetics is, however, also observed for Am(III) and Pu(IV), the origin of which at present is unknown.

The α-autoradiographic study combined with Scanning Electron Microscopy (EDX-SEM) analysis revealed biotite to represent the most important affinity to actinide sorption. As an example the Pu(IV) distribution on a cut sheet of granite is given in Fig. 2-5. Biotite contains Fe(II) which most likely is responsible for the surface enhanced reduction of oxidised actinides. It is well known from the literature that electron transfer is very much enhanced upon surfaces containing Fe(II) as a reductant [Eli1993].

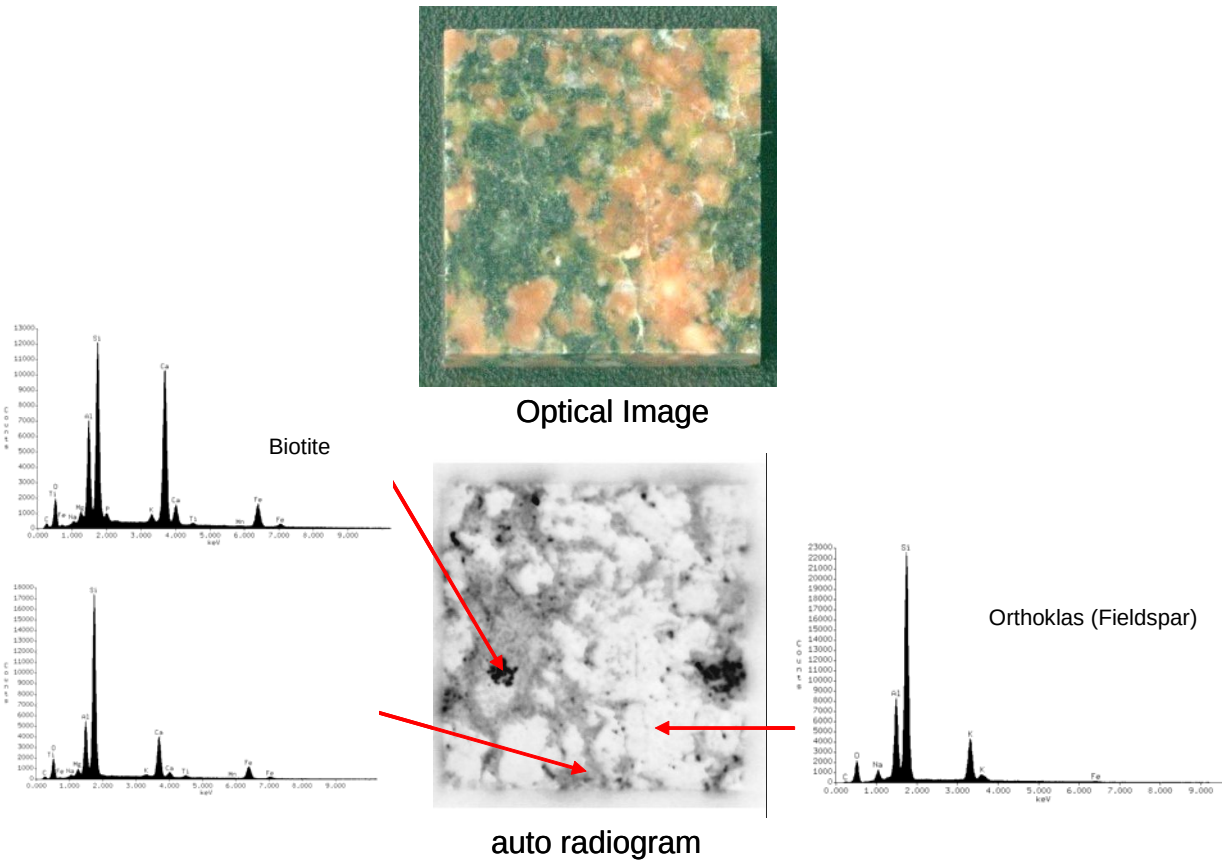

Fig. 2-5 Determination of minerals relevant for Pu sorption.

The dark areas in the α-autoradiograph indicate enhanced Pu-sorption. These areas usually coincide with biotite phases.

For comparison of sorption between the different elements, the sorption coefficient K_s is calculated

$$K_s = \frac{activity\ on\ the\ surface\ (\frac{Bq}{cm^2})}{activity\ in\ the\ solution\ (\frac{Bq}{cm^3})}$$

Results of the sorption experiments (see above) onto freshly broken granite and onto altered material are given in Tab. 2-1.

Tab. 2-1 Sorption coefficient of actinides on Äspö materials after 14 days of exposure

K_s (cm)	freshly broken granite	altered material
^{238}Pu	2.50	1.30
^{237}Np	0.16	0.16
^{233}U	0.026	0.018

Tab. 2-1 shows significant differences between the actinide elements, but only slight differences between freshly broken granite and altered materials. The time dependence of the sorption process within the period under investigation is similar for Pu and U. In contrast Np shows fast sorption onto altered material and retarded sorption onto granite. Np shows similar behavior as U for altered and fresh granite; Sorbed Np is also clearly correlated to some Fe bearing minerals. In contrast, Pu having a significant higher sorption coefficient shows no correlation with the Fe distribution in the slices. Pu is not sorbed homogeneously onto the surfaces, a correlation of sorbed Pu with the element distributions of K, Ca, Si, Al or Mg is not observed.

Sorption behavior of Np and Pu onto natural minerals was determined. Significant sorption of Np was observed onto kryptocrystalline MnO_2 and Fe_2O_3 (var. “kidney ore”). Epidote, titanite and the rough surface of chlorite - cut perpendicular to its cleavage plain - showed also remarkable sorption. However, the smooth surface of tabular Fe_2O_3 and the cleavage plains of phyllosilicates and feldspars showed considerably less sorption.

All mineral species showed much higher sorption of Pu than of Np, but the patterns were similar: Strong sorption of Np and Pu was found on the same minerals. Chlorite showed a comparable sorption dependence with respect to its crystallographic orientation.

2.4 Retention mechanisms and speciation of sorbed actinides

From the investigations presented here, information on the retention mechanism is obtained. In the cocktail injected into the cores, the actinides were present as Am(III), Pu(IV) and Np(V). Comparisons between the actinides showed for core #4 and #5 that Np and Am were retained at the same locations.

Two independent methods were applied for determination of the Np redox state. From slices of core #4, Np was dissolved with HCl and by TTA extraction Np(IV) was separated. As a result, it was found that more than 60% of Np was bound to the slices in the form of Np(IV). Np(V) in solutions, even at negative Eh (e.g. in the cocktail) remained as Np(V) for many months as long as no solids were present. This indicates that solid granite and/or fracture filling material catalyses reductive processes. Potential sites for reduction processes might be pyrite and Fe(II) containing clay minerals which are detected in the Äspö granite.

XPS was applied as another method for identification of chemical valence states of Np and iron. A transfer vessel was used to move samples from the glovebox to the XPS spectrometer (PHI model 5600ci) avoiding air contact. XPS spectra were acquired by use of Mg K_α (1253.6 eV), Al K_α (1486.6 eV) or monochromatic Al K_α X-ray excitation. High-resolution scans of elemental lines were recorded at 11.75 eV pass energy of the hemispherical capacitor analyzer which yields a full-width-at-half-maximum (FWHM) of the Ag $4d_{5/2}$ line of 0.85 eV, 1.02 eV or 0.60 eV, respectively. The energy scale of the spectrometer was calibrated by Cu $2p_{3/2}$, Ag $3d_{5/2}$, and Au $4f_{7/2}$ lines of pure and Ar^+ sputter cleaned metal foils. Analyses at various areas on the samples (from batch experiments) indicated correlation of Np(IV) with the presence of Fe(II). More than 80% of Np could be assigned to the tetravalent state which is confirmed by TTA extraction method.

XPS mapping of a 2mm x 2mm area of granite exposed for 14 days in Np spiked solution showed correlation between Fe(II) and Np(IV) (Fig. 2-6).

XPS measurement was also performed with batch samples exposed to Pu and U. Concentrations of ^{238}Pu are to low for this kind of investigations. Reduction of U(VI) to U(IV) retained on crushed high-FeO olivine rock was reported by Rodrigues at al. using XPS [Rod98]. Due to the groundwater composition used for our experiments, U concentration in the spiked solution was by one order of magnitude lower. This fact and the limited sorption of U (see Tab. 2-1) prevented the detection of U phases by XPS on the surfaces.

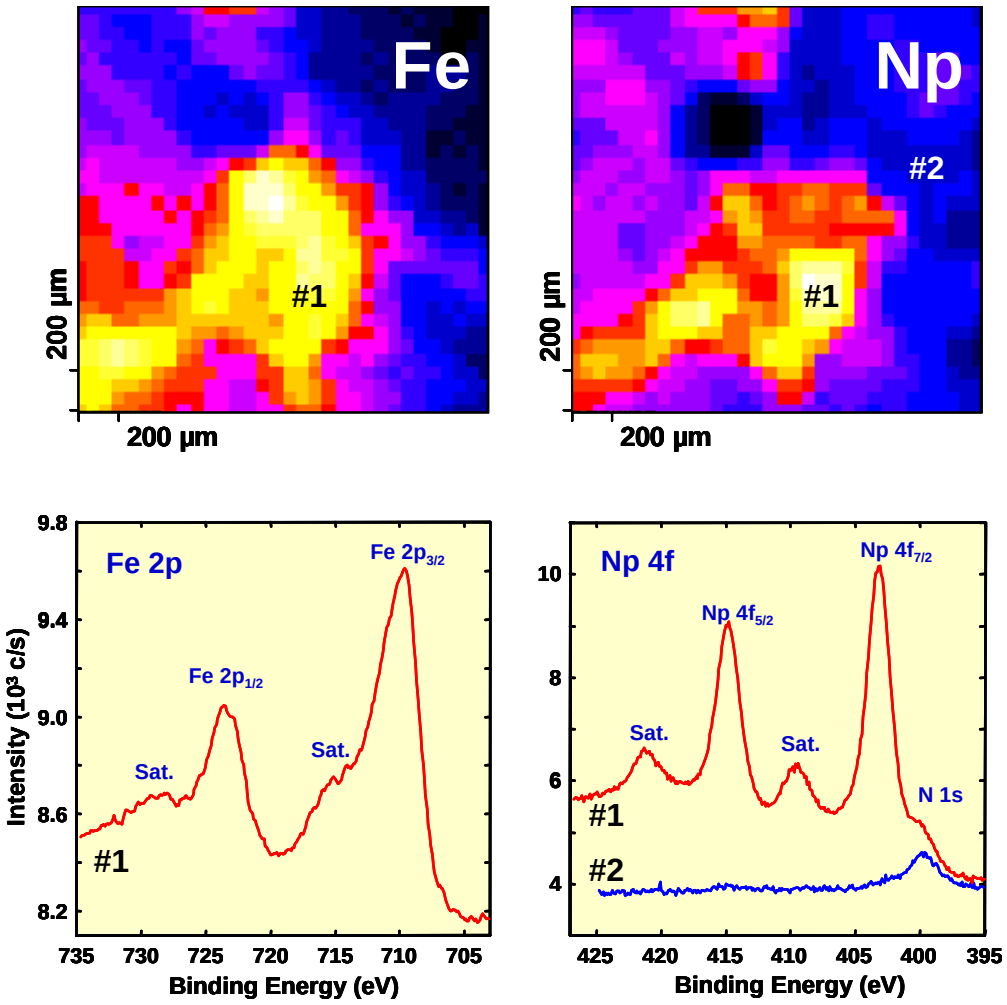

Fig. 2-6 XPS maps of a 2mm × 2mm area of granite exposed for 14 days in Np spiked solution.

(Bright plotted areas correspond to enhanced atomic concentrations) Spectrum #1 and #2 are measured at the locations indicated in the maps.

2.5 Properties of the fractured cores

From drill hole KOV 01 778.50-779.25, three parts could be used for migration experiments. Parts of the core #5, #6. and #7 were placed into cylindrical stainless steel sleeves. The design of these autoclaves is shown in ref. [Kie2003]. The periphery between cores and steel tube wall was filled with epoxy resin. Top and bottom ends were closed with acrylic glass covers. Sealing between the top / bottom ends and the stainless steel sleeve was achieved by O-rings. The lids were provided with fittings for feeding and extracting the groundwater. The length of core #5 was 150 mm and the diameter 52 mm. Tightness of the autoclaves was tested in subsequent laboratory experiments, indicating leak tightness up to 60 bar groundwater pressure. The fluid pressure in CHEMLAB 2 is about 27 bar. The fracture of core #5 was open and not filled with precipitates, whereas in core #2 (to an extreme extend in core #3) and in core #4 the fractures were more or less healed (partly closed).

2.5.1 X-Ray tomography

Prior to the experiments, the internal structures of the embedded drill core were investigated by means of nondestructive X-ray tomography. This procedure was previously applied also to core #3 [Vej2001].

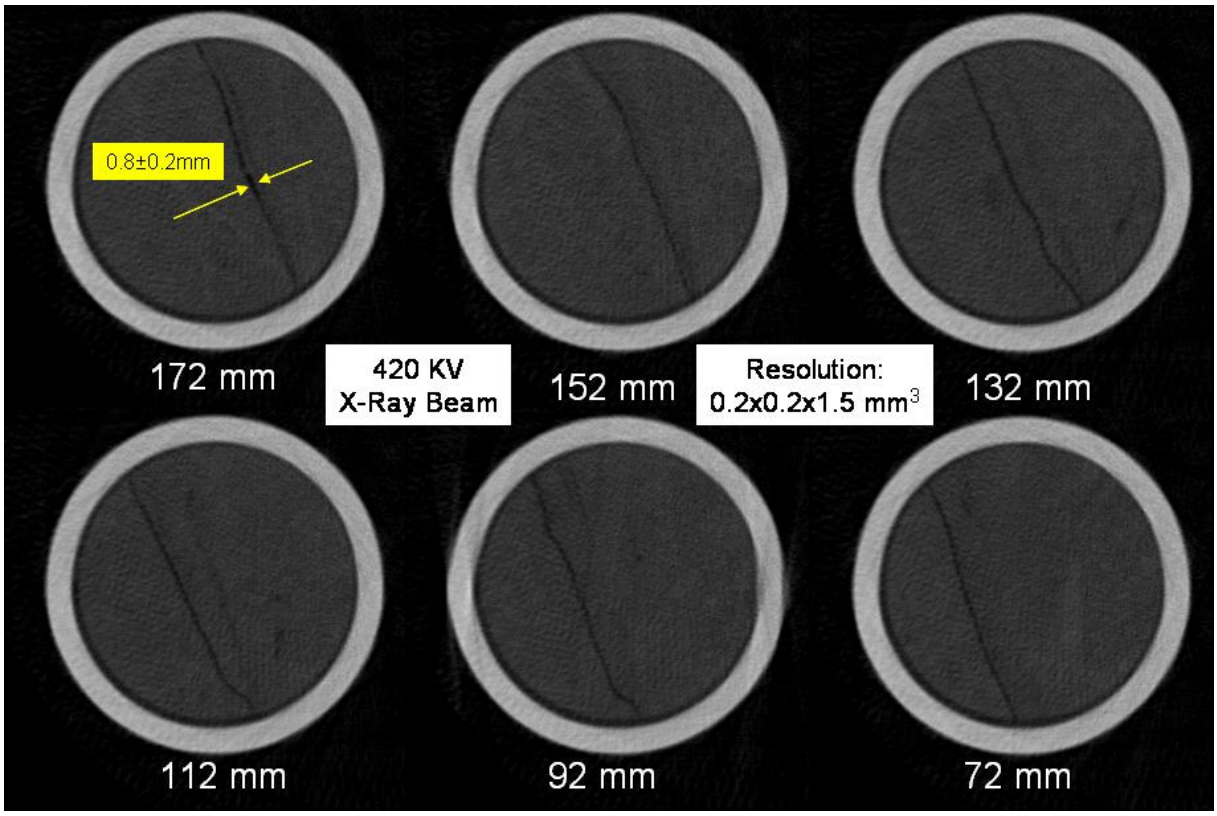

Fig. 2-7 Images of X-ray tomography analysis of core #5

X-ray computer tomography[a] was applied to core #5, #6 and #7. As radiation source a 420 kV X-ray tube, having a focus diameter of 1.5 mm was applied. Measurements were performed by 15 detectors at collimator sizes of 0.8x1.5 mm. Evaluated volume elements of the core had a volume of 0.2x0.2x1.5 mm^3. By these investigations, about 100 images of horizontal cross sections of each core were produced. In Fig. 2-7, dark areas indicate lower densities. Continuous flow paths are found in all cores. The steel mantle, the epoxy resin between steel autoclave and granite material as well as internal structures can be seen clearly. The aperture for the fracture in the core #5 was determined to be in the range of 0.8 mm.

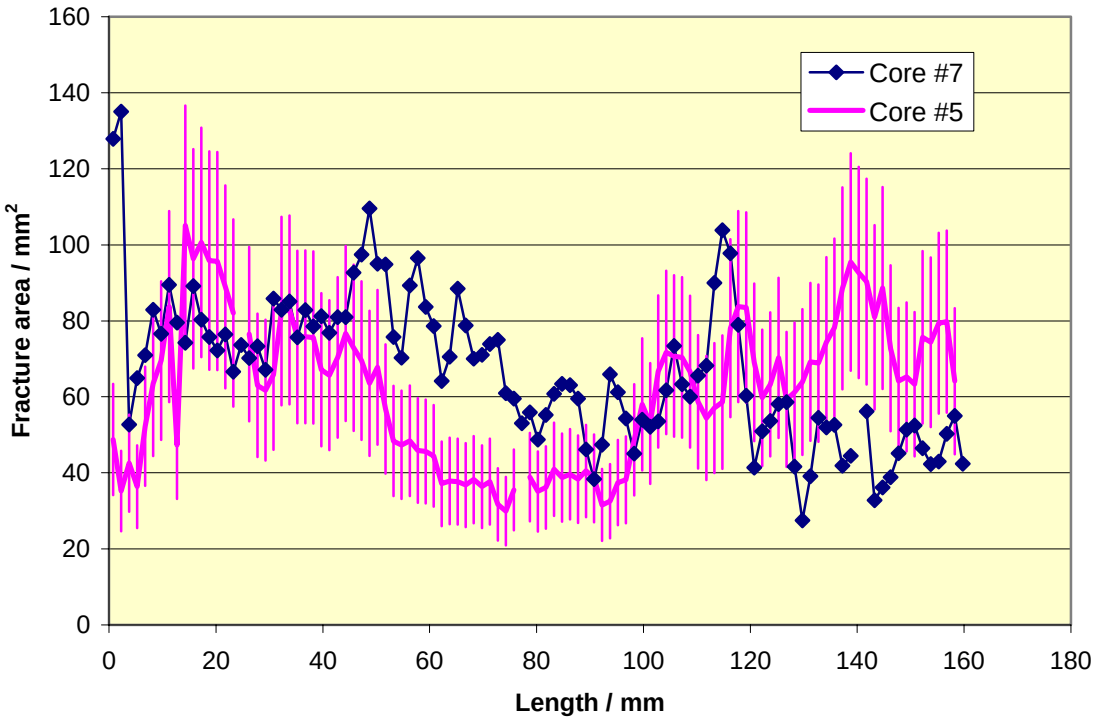

Fig. 2-8 Fracture sizes of the cores #5 and #7 determined by evaluation of X-ray tomography data.

Vertical lines (core #5) represent error bars, derived by variation of the threshold values for distinguishing between dark grey and black colour in tomography data.

By evaluation of the images from X-ray tomography, fracture sizes of the cores #5 and #7 were determined. Determination was done by means of the Mathcad 2001 software, the images were processed and threshold values were applied in order to distinguish between the dark grey colour of the solids and the black colour of the fracture. By variation of the threshold, errors of these measurements could be deduced which are indicated in Fig. 2-8.

[a] X-ray tomography including graphical representation was performed by Bundesanstalt für Material Forschung in Berlin (BAM)

For core #5, the maximum open fracture areas up 100 mm^2 to are located at a distance between 14 mm and 23 mm and at 140 mm. Minima of open fracture areas occur in the range from 53 mm to 98 mm providing areas below 40 mm^2.

2.5.2 Analyses of local flow pathes

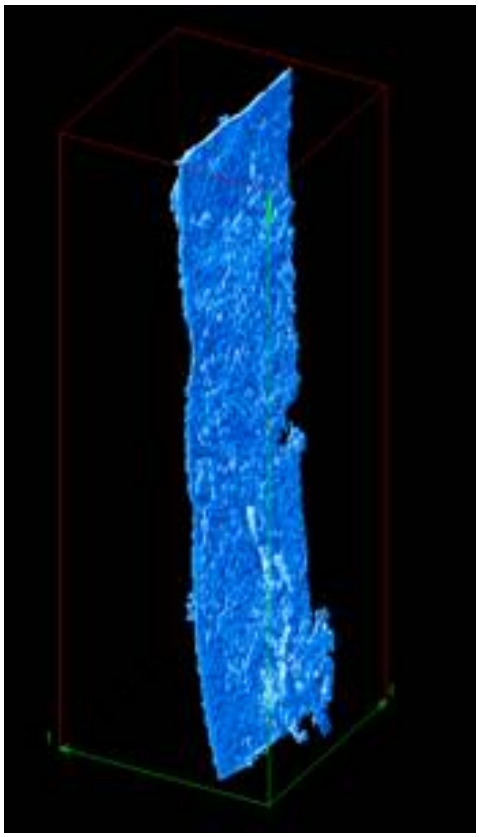

Fig. 2-9 3 D (voxel) representation of a fracture in core #5 determined from X-ray tomography data.

The geometry of the flow path has fundamental influence for all flow and transportation processes (in all scales). The local flow path area is obtained by processing of the data from the computer tomography. The result of this processing is a three-dimensional structure of the internal (pore) area of the flow path.

For transportation processes only the area is of interest which is actually involved in the flow and transportation processes, frequently called the effektive pore volume. This effective pore volume is computed in the model by means of percolation algorithms resulting in a reduced pore structure. Effective transport parameters are derived such as porosity and specific surface from the geometrical structural data.

This data set (shown in Fig. 2-9) will be used as a basis of forthcoming work to the development of a transport modelling approach appropriate to describe the measured actinide migration. For the spatial structure, the flow can be computed by a Lattice Boltzmann method. The resulting zone of flow corresponds to a specific solution of the Navier Stokes equation. The hydrodynamic dispersion is not needed for these kind of computations, since the dispersion is contained in the heterogeneity of the flow path. Radionuclide transport can be computed by application of a Monte Carlo particle method. The substantial difference to conventional (macroscopic) transportation models is that only one advection term (3-D zone of flow in the fracture) and a molecular diffusion term (Monte Carlo implementation) are needed.

The Fig. 2-9 and Fig. 2-10 show the complexity of fracture geometry in the drill cores. Especially in core #7 the fracture is splitted, showing a very complex percolation structure where radionuclide migration will take place.

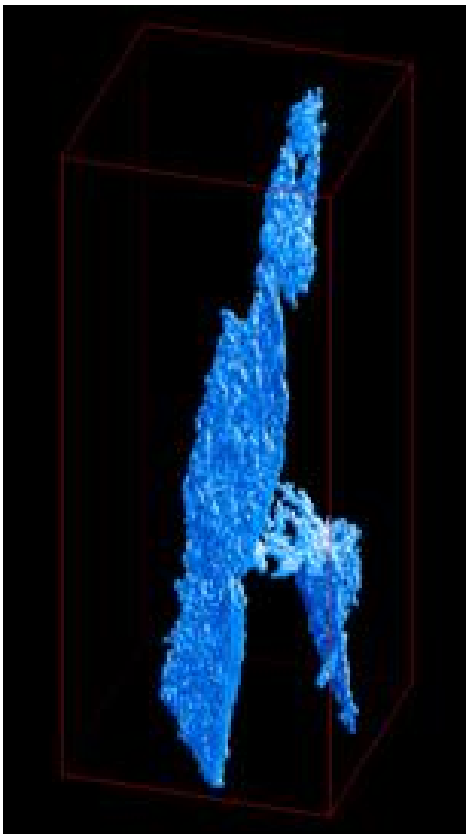

Fig. 2-10 3 D (voxel) representation of a fracture in core #7 determined from X-ray tomography data.

2.5.3 Hydraulic properties of core #5

Hydraulic properties, such as effective porosity, dispersion coefficient, breakthrough time are determined by evaluating measured breakthrough curves of non sorbing tracer like HTO. HTO breakthrough curves were measured applying flow rates between 0.1060 ml/min and 0.0047 ml/min. Pulse injection of about 50 µl of HTO solution was applied. Background subtraction is performed by defining a minimum HTO concentration of the breakthrough peak. Breakthrough curves for HTO are shown in ref. [Vej2001]. The zeroth, first and second order momentums of the time dependent breakthrough curves are computed corresponding to the evaluation given by Appelo 1994.

The hydraulic data are evaluated as described in [Vej2001]. The results are shown in the Tab. 2-2. Dividing the Darcy velocity determined from the flow rate by the pore water velocity v_0, the effective porosity of the core in volume units is obtained. The porosity value given in the table relates the effective porosity to the total volume of the core.

It can be seen from the table that in spite of a variation of the flow rate by a factor of about 20, the dispersion coefficient, the porosity and the Peclet number are similar.

Tab. 2-2 Hydraulic properties of core #5

Flow rate		**0.106 ml/min**	**0.047 ml/min**	**0.0047 ml/min**
l	m	0.15	0.15	0.15
t_0	s	1448±323	3954±919	30097±6840
v_0	m/s	$(1.04\pm0.23)\times10^{-4}$	$(3.79\pm0.88)\times10^{-5}$	$(5.01\pm1.14)\times10^{-6}$
σ^2_t	-	1.090	1.088	1.12
D	m^2/s	8.48×10^{-6}	3.07×10^{-6}	4.19×10^{-7}
α	m	8.17×10^{-2}	8.08×10^{-2}	8.36×10^{-2}
Pore Volume	ml	2.6±0.6	2.7±0.6	2.3 ±0.5
Porosity	%	0.82	0.85	0.72
Peclet Number	-	1.84	1.54	1.79

The HTO elution curves of these experiments are shown in Fig. 2-11. The vertical dotted lines represent the computed breakthrough from momentum analysis given in Tab. 2-2. These data take into account the tailing of the curves.

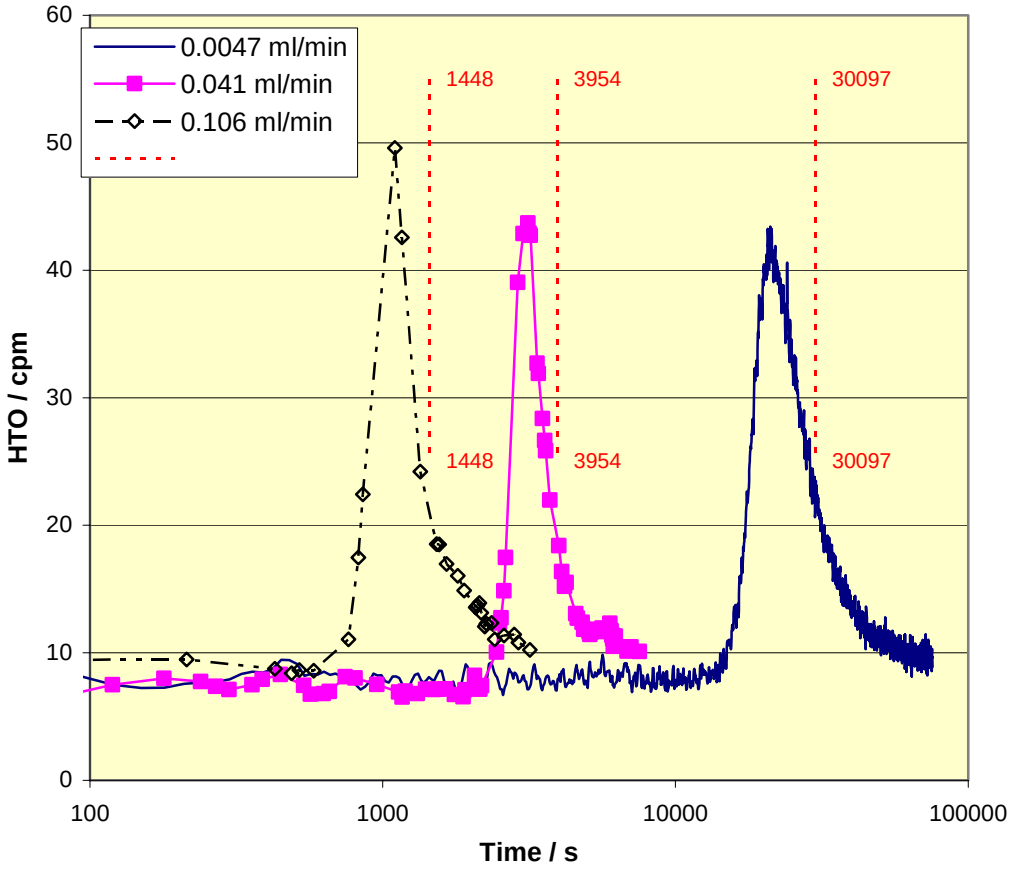

Fig. 2-11 Elution curves of inert HTO tracer for determination of hydraulic parameters of core #5.

3 Actinide Migration Experiment in CHEMLAB 2

The experiment with core #5 was the third in-situ actinide migration test performed with the CHEMLAB 2 probe at Äspö HRL. The second in-situ migration experiment with core #3 was started in November 2001. The fracture of core #3 was clogged by precipitates to a large extend. Consequently, this core showed a very low hydraulic conductivity. A low flow rate of 0.03 ml h^{-1} was selected, the duration of this experiment was scheduled for 3 month. Due to a defect of the CHEMLAB 2 probe, the experiment was interrupted during the actinide cocktail injection phase. A breakthrough of HTO or actinides could not be measured due to the short injection period. However, the core #3 was contaminated by actinides and had to be treated accordingly.

It required some time to readjust the CHEMLAB probe. The next in-situ experiment was started at November 27, 2002. The actinide cocktail was prepared as described in the previous publications. CHEMLAB 2 was prepared with the core #5 in the autoclave and the reservoir containing the actinide cocktail. CHEMLAB 2 was inserted into the drill hole, coupled to the glove box and a test run was started. It was intended to use a constant flow rate (0.04 ml h^{-1}) comparable to the one chosen for the previous test. The experiment should kept running for 3 month minimum. By the CHEMLAB 2 control system, the actinide cocktail from the reservoir was injected for 10 days (until December 7, 2002). The composition of the cocktail is given in Tab. 3-1. Afterwards, natural groundwater of the CHEMLAB 2 drill hole was pumped. However, a technical problem of the CHEMLAB 2 probe caused fluctuations in the flow rate. Fig. 3-1 shows that the pressure at the packer dropped by more than 10 bars within the first days, and during December 2002 several collapses were recorded. Significant fluctuations showed the pump pressure, too. After about 45 days (January 8, 2003), the test was interrupted and CHEMLAB 2 recovered. The probe could be fixed and the test was continued at a higher flow rate of 0.3 ml h^{-1} from February 12 until April 8, 2003. Afterwards, the core and the eluted groundwater samples were transferred to FZK-INE for analysis.

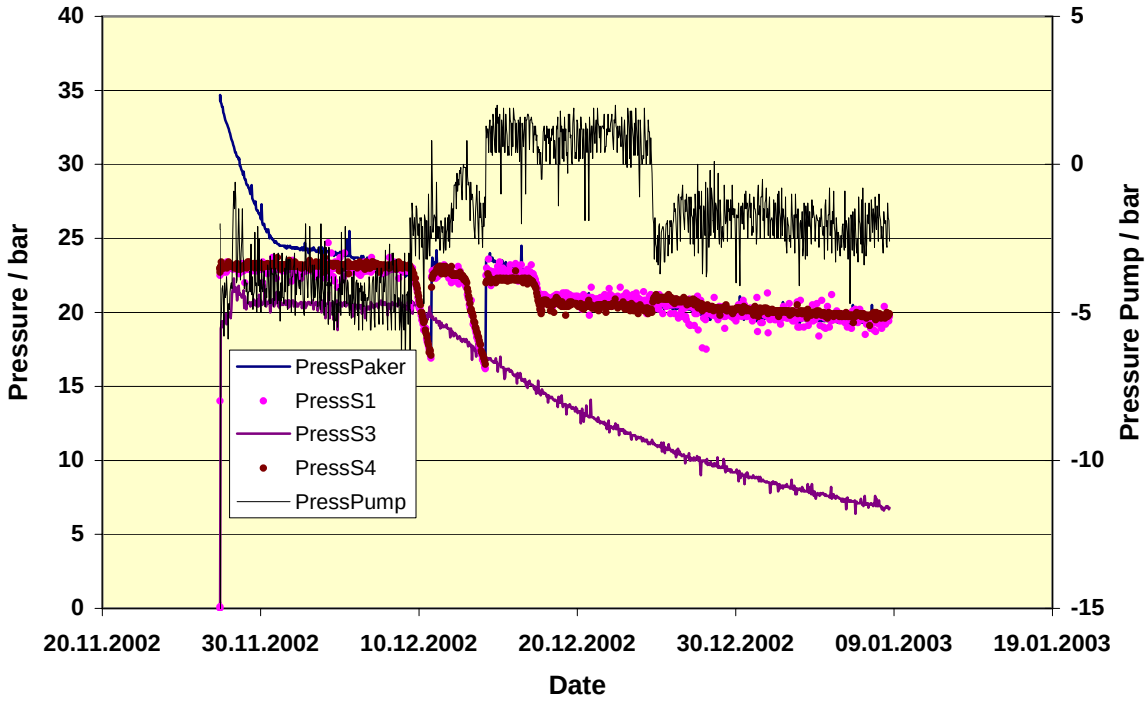

Fig. 3-1 Pressure log of CHEMLAB 2 during the first phase of the experiment

Tab. 3-1 Composition of the actinide cocktail (50 ml) used for the CHEMLAB experiment with core #5

Nuclide	**Activity of the cocktail (50 ml)** Bq / 50 ml	**Impurities** Bq / 50 ml	**Concentration** mol / L
HTO	$9x10^{3}$		
^{237}Np	$3.3x10^{3}$		$1.1x10^{-5}$
^{242}Pu	$1.7x10^{2}$	^{238}Pu: 38 ^{239}Pu: 15	$9.7x10^{-8}$
^{243}Am	$8.0x10^{2}$	$^{243/244}Cm$: $1.5x10^{3}$	$8.9x10^{-9}$

The volume of the tubing[b] between CHEMLAB 2 and the glove box in the tunnel (20 m) is about 8.8 ml. Sampling was performed at a rate of one sample per 30 h. Until January 8, 36 samples comprising 34 ml were collected, after the restart of the experiment in February, 175 ml of groundwater were eluted and collected in one single sample.

After termination of the experiment, the reservoir with the remaining cocktail volume was returned to FZK-INE. Between preparation and return of the cocktail, some 10 months passed. In this period, the concentrations changed. The differences are given in Tab. 3-2.

Tab. 3-2 Variation of the composition of the actinide cocktail between preparation and return

Nuclide	**Activity of the cocktail** **21 October 2002** Bq / ml	**Activity of the cocktail** **21 August 2003** Bq / ml
^{237}Np	66	40
^{241}Am	0.06	
^{243}Am	16	2.2
$^{243/244}Cm$	31	4.7

Tab. 3-2 shows that the concentration of americium and curium was reduced by a factor of 7. If this reduction is attributed to sorption or precipitation in the reservoir is not yet clear.

Following results are obtained from the 3rd actinide experiment in CHEMLAB 2.

[b] Length of the tube: 20 m, inner diameter: 0.75 mm

3.1 Eluted groundwater and breakthrough of tracers

The eluted groundwater was collected by a sampler. The samples were kept sealed hermetically to avoid evaporation of water. The volume of eluted groundwater was determined by balancing the samples. As a consequence of the fluctuations of the groundwater flow in CHEMLAB 2, the HTO breakthrough curve shows disruptions, too (see Fig. 3-2). Due to the fluctuations of the flow rate, during the injection period from November 27 until December 7, 2002, in total 7.8 ml of spiked cocktail was injected into core #5.

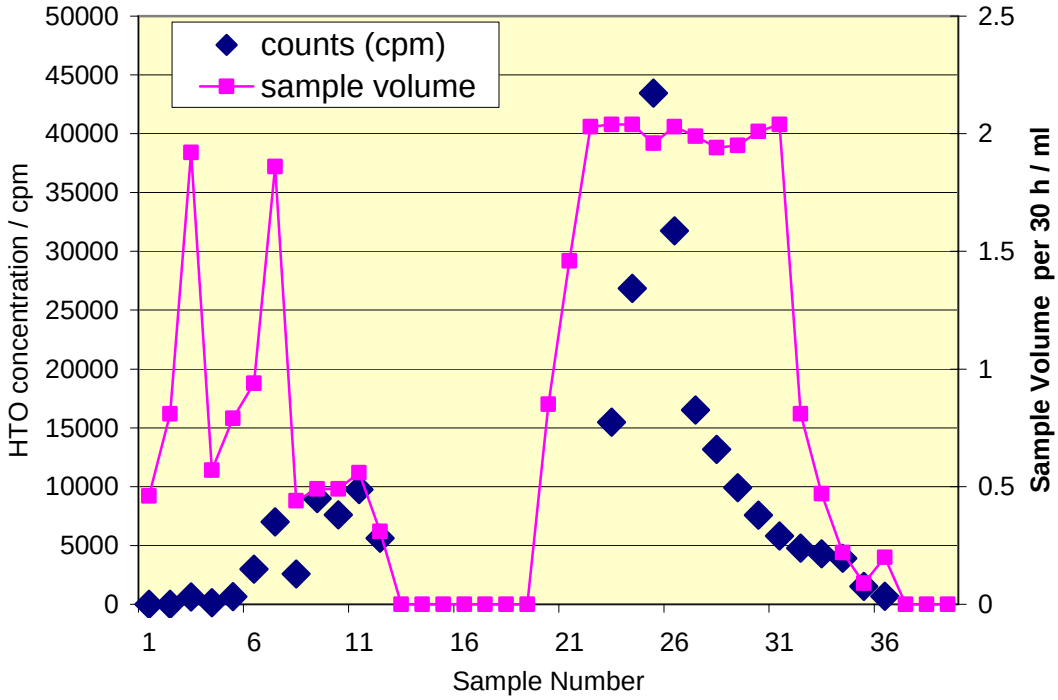

Fig. 3-2 HTO breakthrough in the in-situ experiment with core #5

Hydraulic data could be obtained from breakthrough of HTO: Mean residence time of the tracer in the core was 744 ± 6 hours, σ^2_t is 1.05 and α is 7.88×10^{-2} m. These data agree excellently with those determined in laboratory (Tab. 2-2). With respect to the disruption of the flow, it is not possible to derive the mean flow rate and the total porosity from this breakthrough curve.

Integrating the sample volumes, the breakthrough depending on the eluted volume could be obtained (Fig. 3-3). In the single sample collected after February 12, 2003, in total 230 Bq of HTO were found.

The recovery of HTO is calculated from the sum of the total measured HTO activity divided by the activity injected in core #5. However, due to the fact that some sampling vials were completely filled, evaporation of eluted water cannot be excluded to some extend. This may be relevant for those samples having more than 2 ml in Fig. 3-2. By comparison of the recovered HTO activity with the initial HTO concentration in the cocktail, the total volume of injected cocktail may be underestimated by about 37 %. Cumulated error for the determination of eluted volume results in a range from 34 ml to 46 ml.

Actinides could not be detected in the eluted groundwater, neither by LSC nor by ICP MS techniques.

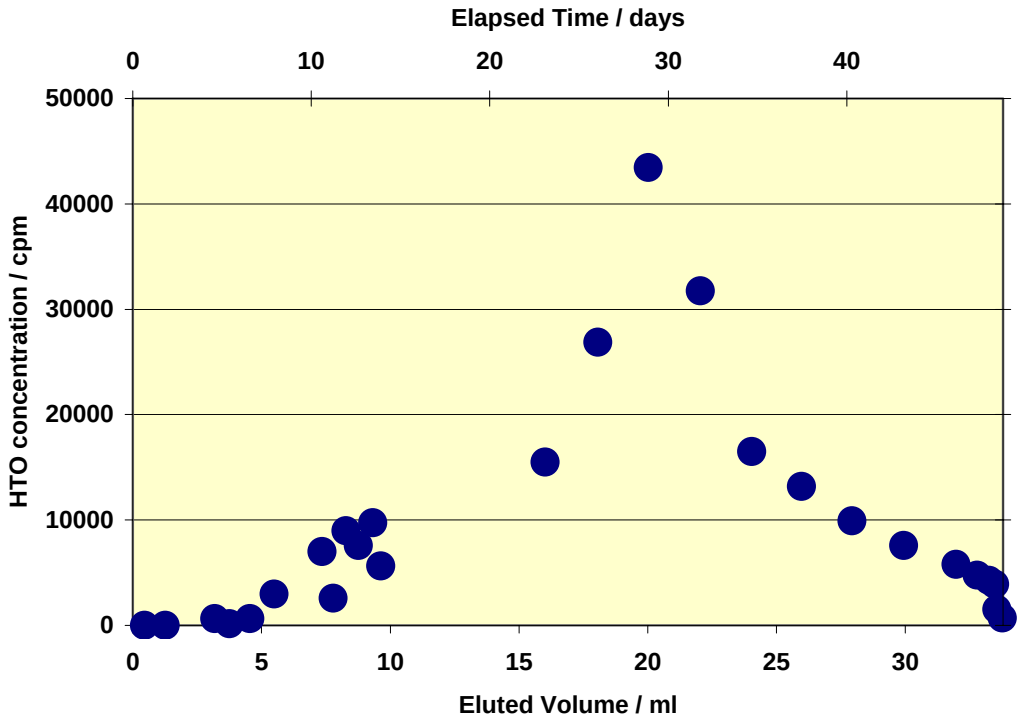

Fig. 3-3 HTO breakthrough curve as function of the eluted volume for core #5 in the CHEMLAB 2 experiment

Cumulated error of eluted volume: 34 ml to 46 ml

3.2 Post mortem investigations of core #5

Investigations of the flow path of core #5 were performed as described previously [Kie2003]. A fluorescent epoxy resin [Fri98] (Component A: epoxy resins + dye (Fluorol yellow-088, BASF) Component B: amine-hardener (modifed alphatic polyamine), Viscosity: 100 mpa s (23 °C)) was injected into the fracture after drying the system by injection of isopropanol.

After hardening of the fluorescent epoxy resin, the core was cut perpendicular to the cylinder axis by means of a 0.7 mm thick diamond cutting blade. The resulting slices had a thickness of 4 mm.

The geometry of the flow path was analyzed by scanning the slices and discrimination of colors with respect to the fluorescent resin. The volumes and the inner surface areas of the fracture were determined from the scans by means of pixel counting and numerical evaluation. The radioactivity of the slices was measured by a α-autoradiography instrument using α- and β-sensitive sheets. As described in ref. [Röm2002], the α-autoradiography and the optical information of the slices were combined.

The abraded material from the cuts was sampled, dissolved and prepared for ICP-MS element analysis and γ-counting.

3.2.1 Actual flow path

Analyses of the distributions of the fluorescent resin in each slice were compared with the results of X-ray tomography and the corresponding distribution of α-tracks in the autoradiography. From the slices, the total area of colored epoxy resin was determined. As to be seen from Fig. 3-4, some deviations between the non destructive and post mortem flow path analysis occurred.

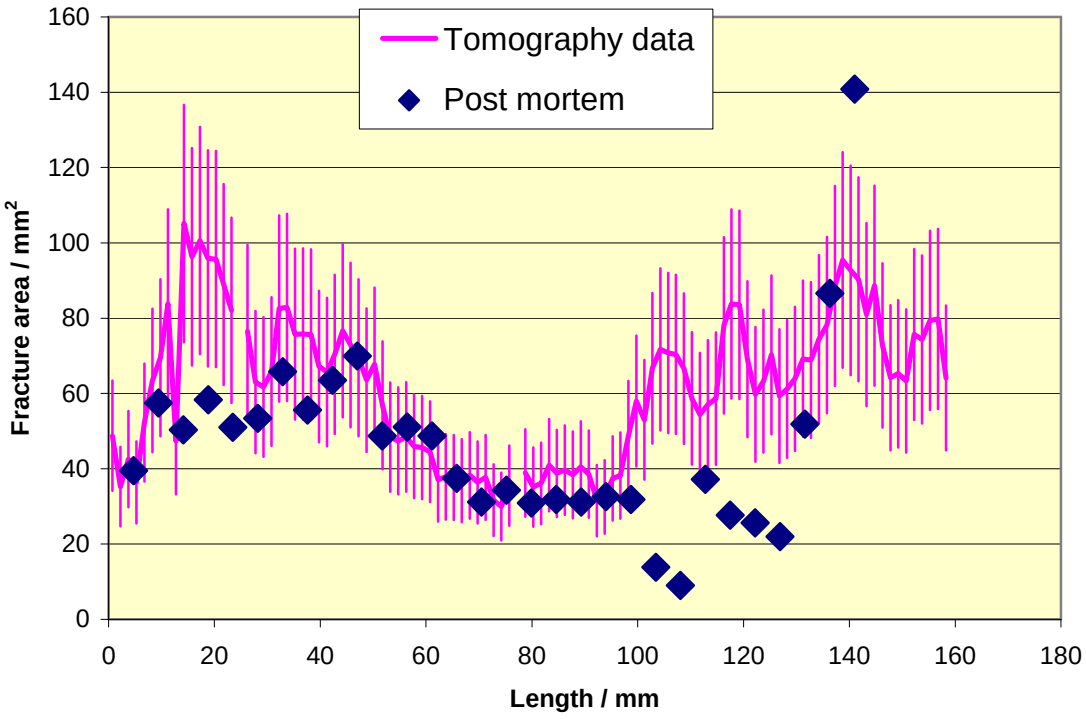

Fig. 3-4 Comparison between fractures area determined by X-ray tomography and post mortem investigations. (Analysis of fluorescent resin the slices)

In the region between 30 and 100 mm of core #5 both detection techniques agreed well. In the ranges between 20 and 30 mm and from 100 mm to the end significant discrepancies are observed. Detailed analyses of the tomography data showed, that in these ranges parts of the core provided lower densities which were attributed to the fracture.

3.2.2 Distribution of radioactivity along the flow path

As in for the previous experiments, different detection techniques were applied for sorbed actinide elements along the flow path. At first, the total α-activity was measured by α-autoradiography (see Fig. 3-5).

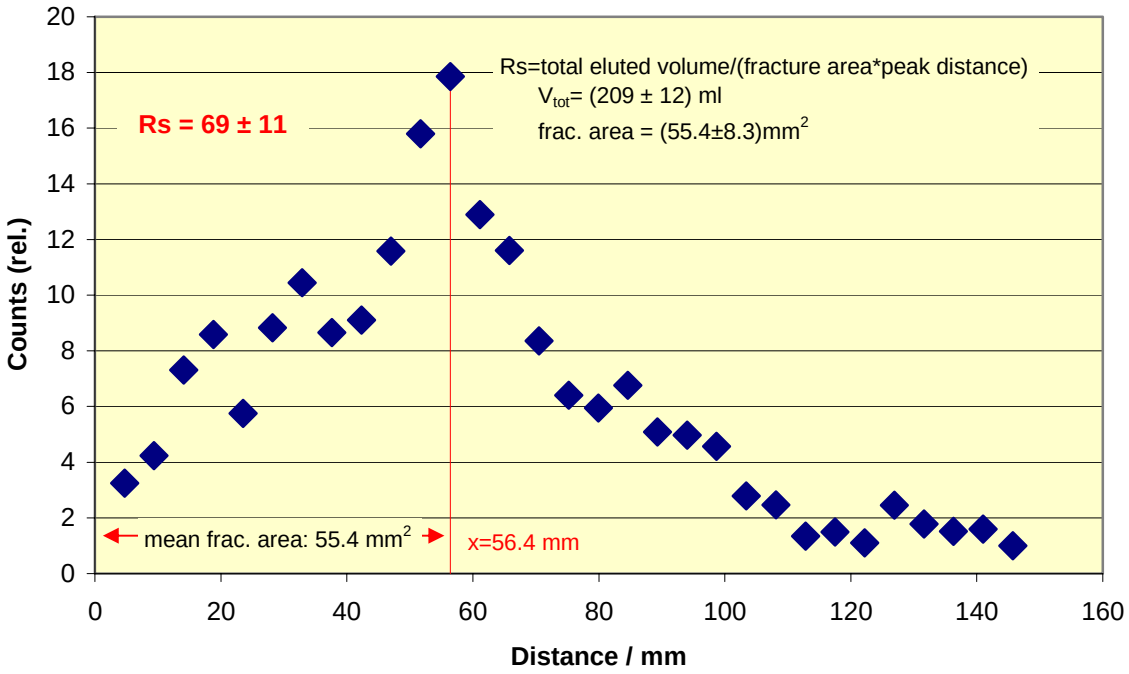

Fig. 3-5 Distribution of (relative) α-activity in the slices, measured by α-autoradiography

Complete α-activity stuck in core #5 up to 110 mm. From this method it could not be distinguished between the different elements. Taking the maximum distance of the distribution from the injection a retardation coefficient could be derived. Following assumptions are considered: R_s is the ratio between the ground water velocity (represented by the inert tracer) and the migration velocity of the actinides. As the inert tracer is eluted completely, the groundwater velocity is computed by

$$v_w = \frac{Volume_{eluted}}{area_{fracture} \cdot time} \qquad (3.1)$$

where the mean fracture area is computed from the resin distributions of the slices. The migration velocity is given by

$$v_{actinides} = \frac{\text{distance of peak}}{\text{time}} \qquad (3.2)$$

X_{peak}: distance of peak

$$R_s = \frac{v_w}{v_{actinides}} = \frac{Volume_{eluted}}{area_{fracture} \cdot X_{peak}} \qquad (3.3)$$

For data shown in Fig. 3-5, $R_s = 69 \pm 11$ is calculated. The error is not a statistical one, but it takes into account the error in the determination of the eluted volume.

3.2.3 Element profiles

As reported in previous papers, depositions of ^{243}Am and ^{237}Np were determined by two different methods: γ-counting of ^{233}Pa (daughter of ^{237}Np) in the slices and dissolution and subsequent ICP-MS analysis of the abraded material from cutting the slices.

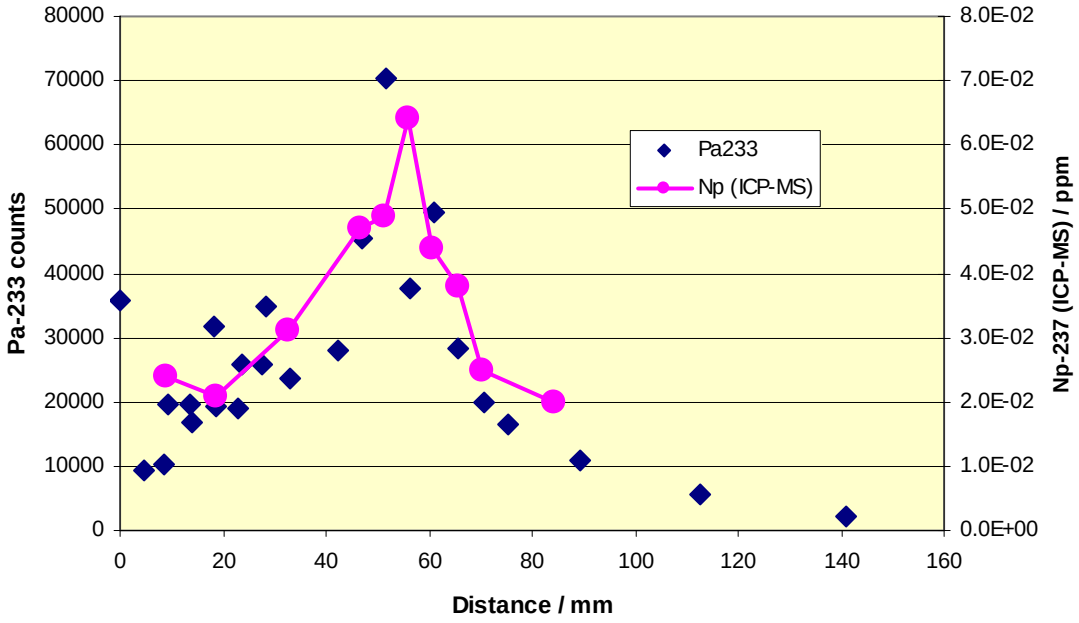

Fig. 3-6 Correlation of the ^{237}Np concentrations determined by γ-counting and by dissolution and ICP-MS analysis

This figure (Fig. 3-6) shows that both methods produced consistent results which agreed also with the α-autoradiography data (see Fig. 3-5). Am could not be detected by ICP-MS measurements. From γ-counting of Am, the distribution of this element was determined and is shown in Fig. 3-7. Due to the different γ-decay schemes, the absolute count rate for Am is

lower by a factor of 40 than in the case of Np. For this reason, the distribution shows a significant scatter, however, the maximum measured decay rate was found in the same region as the Np peak.

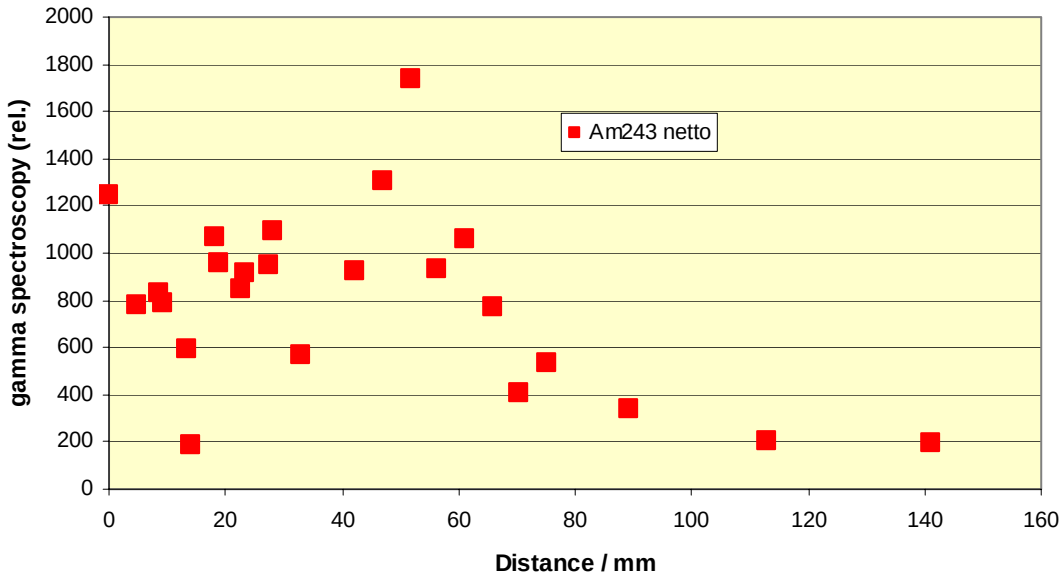

Fig. 3-7 Am concentrations determined by γ-counting of the slices

4 Discussion

4.1 Comparison to the breakthroughs of previous experiments

Laboratory migration experiments using core #1 were run with pulse injections at flow rates between 3 and 0.06 ml/h. In 9 successive actinide migration experiments with core #1, the radionuclide concentrations in the eluate were determined by both α-spectroscopy and ICP-MS measurement. The migration of Np was retarded compared to the migration of HTO; the breakthrough peak occurred at approx. 3 - 4 ml of eluate as compared to 1.7 ml for the HTO breakthrough curve. Recoveries for ^{237}Np were between 20 and 40% for flow rates of 3 ml/h, and between 5 and 15% for flow rates of 0.06 ml/h. These results showed that the bulk of Np was retained, especially at low flow rates. Np concentration in the eluate (core #1) did not exceed approx. 4×10^{-8} mol/L.

With core #4, three subsequent actinide experiments were performed in laboratory injecting 14 mL of actinide cocktail at constant flow rate of 0.3 mL/h. Breakthrough of HTO and actinides was recorded by collecting about 40 drops per sample (0.96 mL). Only in the first experiment with core #4, a breakthrough of Np was observed. In the following tests, Np was found in concentrations of 0.06 and 0.2 µmol·dm^{-3} close to the detection limit. Am and Pu concentrations in the eluated water were below detection limit. HTO tracer was detected al-

ready in the first fraction. The maximum HTO concentrations were observed in the samples between 4.8 and 14.4 ml and 3.8 and 13.4 ml, respectively.

The same injection scheme was applied in CHEMLAB 2 with core #2. Results and comparisons between these experiments are reported elsewhere [Kie2002a], [Röm2002]. In both experiments, the breakthrough of Np followed the tendency of the HTO curve. In laboratory experiments as well as in the in-situ experiment, breakthrough of Np is observed to be unretarded compared to the inert HTO tracer. Recovery of Np in the core #4 experiment was about 26 %, whereas in the CHEMLAB experiment 40 % of Np was recovered. In the peak of the breakthrough of the CHEMLAB 2 experiment, speciation of Np was analyzed by absorption spectroscopy. The spectrum showed only one absorption band to the free NpO_2^+. Using the known absorption coefficient, the NpO_2^+ concentration corresponded to the total Np measured by liquid scintillation counting, indicating the absence of colloids and carbonate complexes [Kie2003].

4.2 Comparison to actinide distributions from previous experiments

Similar to core #5, core #1 showed an open fracture of an average aperture of 0.8 mm. Core #2 and #4 showed partly open fractures at both ends. In core #2 and #4, visual inspection showed no open fracture and parts of both cores were completely clogged. Structures which could be seen in the scans of core #2 and #4 slices were attributed to a healed fracture system. Volumes of core #2 filled with fluorescent resin were generally too small to be identified by the fluorescence scanning technique, however, single spots of fluorescent resin could be identified visually throughout many slices of the core. Core #4 could not be penetrated by the epoxy resin. Core #3 which was used in an unsuccessful CHEMLAB experiment was completely clogged by precipitates.

After impregnation of the fractures with a fluorescent resin and cutting, volumes and inner surfaces of the fracture were determined by scanning and pixel counting of the slices. The open fracture of core #1 was oriented in a small angle to the cylinder axis. The core was analyzed from the point of injection to a distance of 56.4 mm. In this range, the open fracture cross sections varied between 38 and 87 mm^2 (mean value 53 mm^2) and the circumferences of the fracture at top and bottom of each slice were determined between 72 and 96 mm (mean value 80 mm). In the case of core #5 the average cross section of the fracture for 30 slices amounts to 46.3 $\pm$ 24.8 mm^2. The variation of the cross sections in core #5 was between 9 and 87 mm^2.

Actinide concentrations retained in each 4 mm slice were measured. α-autoradiography resulted in a strong correlation of the sorbed radioactivity with the surfaces of the fracture especially for core #1 and #5 where open fractures existed. Sorbed actinides in cores #2 and #4 are not directly associated to visible fractures. For interpretation and comparison of the data obtained for core #4, one has to keep in mind, that 3 distinct experiments were performed with this core. The recovery measured for ^{237}Np varied between 40% in the CHEM-

LAB 2 experiment and 26% in the first laboratory experiment. Further laboratory experiments with core #4 showed no recovery of actinides.

Due to the three different experiments, a higher Np content was found in the abraded material of core #4 than for core #2. The distribution of Np in core #4 showed the highest values directly at the injection (distance 0 to 4 mm), a first peak at a distance between 30 and 40 mm and a 3rd less pronounced peak between 104 and 118 mm. All these peaks were indicated by several measurements of abraded material as well as by γ-counting of ^{233}Pa (daughter of ^{237}Np). In the CHEMLAB core #2, a broad Np distribution between 50 and 112 mm was recorded.

The 3 peaks in the spatial distribution of Np were also found in the ^{243}Am distribution at almost the same locations. In core #4, highest ^{244}Pu concentration could be detected at zero distance. At the distance of 30 mm, a single measurement surmounts the concentrations found in adjacent slices. At distances greater than 40 mm, ^{244}Pu concentration in the abraded material was below detection limit. For core #2, ^{243}Am and ^{244}Pu was everywhere below the detection limit of 0.3 pmol/g (0.07 ng/g).

Slices of both cores were analyzed by means of α-autoradiography and the α-distribution was compared with optical scans of the slices. In both cores, complicated distributions of retained α-emitters were found. At the maximum, Np activity in core #2 accounts to 5 Bq/g and to 20 Bq/g for core #4. The spatial patterns obtained by α-autoradiography were not necessarily correlated with fracture filling material which could be discriminated from granite by its color. The spatial resolution of α-autoradiography was constrained by the natural radioactivity arising from the U and Th content of granite. These elements are in equilibrium with their decay chain, including β-emitters. For the cores, the total number of Np decays was in the same range as the number of α-decays produced by natural decay chains of U and Th.

From core #4 experiments, a lower limit for the retardation factors for Am and Pu can be estimated. By comparing the open volume of the fracture to the total groundwater volume eluted during the 3 consecutive experiments, a retardation coefficient R_s = 135 was obtained.

In core #5, both ^{237}Np and ^{243}Am distributions show the maximum count rate at a distance between 51 and 56 mm from injection. The maximum of Np was verified by both detection methods. However, the maximum for Am is characterized only by very few data points showing a wide scatter. ^{242}Pu could not be detected by ICP-MS. Further analyses with respect to plutonium are presently under preparation. From core #5 experiments, a lower limit for the retardation factors for Np and Am is estimated by comparing the location of the Np peak with the total groundwater volume eluted (see Fig. 3-5). A retardation coefficient R_s = 69 is obtained which is by a factor of 2 below the R_s coefficient determined from core #4. The difference may be attributed to the fact that in core #5 an open fracture system existed and therefore the specific surface area per migrated distance was significantly lower than in the almost clogged core #4.

4.3 Comparison to sorption behavior determined in batch experiments

Tab. 2-1 shows significant differences between the actinide elements, but only slight differences between freshly broken granite and altered materials. The time dependence of the sorption process within the period under investigation is similar for Pu and U. In contrast Np shows fast sorption onto altered material and retarded sorption onto granite.

Following relation can be obtained for the retardation coefficient R_s:

$$R_s = \frac{mass_{sorbed}}{mass_{dissolved}} = \frac{c_0 \cdot K_s \cdot surface_{fracture}}{c_0 \cdot volume_{fracture}} = \frac{K_s \cdot f}{\delta} \qquad (4.1)$$

R_s: retardation coefficient
c_0: dissolved concentration
K_s: sorption coefficient (surface related)
f: form factor for surface area
δ: aperture of the fracture

The form factor for surface area includes deviations of the actual surface and void volume of the fracture from the calculated geometrical properties. Combining the Np sorption data with the information obtained from sorbed Np in core #5 (see Fig. 3-5), a form factor for the surface of 21.5 is calculated. Using this value together with the sorption coefficient for Pu (Tab. 2-1), a retardation coefficient of 1075 for freshly broken granite and 560 for altered material is obtained. Taking as basis the distance of the Np peak at about 56 mm, the Pu peak is expected at a distance of 4 to 7 mm from the injection.

5 Conclusions and Outlook

Following conclusions can be drawn from this study:

- Np is retained onto granite and altered materials by reduction to Np(IV) in presence of Fe(II) minerals.

- Pu sorption takes place on a multitude of minerals. Specific sorption processes cannot yet be presented. However, the sorption coefficient is significantly higher compared to Np or U in agreement with migration experiments.

- From the location of the Np peak in core #5 at 56 mm, a Pu peak is expected at about 4 to 7 mm from the injection. This finding shows that Pu was almost immobile within the core #5 experiment. To prove this finding, the first slice of core #5 will be analyzed for Pu by additional methods.

The next CHEMLAB experiment is planned with core #7 using U and Tc as tracers. From sorption data presented inTab. 2-1, U migration is increased by a factor of 6 compared to Np.

This means that for the same flow rate as it was intended for the core #5 experiment and assuming similar properties of the flow path of core #7, a breakthrough is expected after injection of 15 ml.

Acknowledgment

The work was performed within the Project Agreement for collaboration on certain experiments related to the disposal of radioactive waste in the Hard Rock Laboratory Äspö (HRL) between the German Bundesministerium für Wirtschaft und Arbeit (BMWA) and Svensk Kärnbränslehantering AB (SKB).

The authors thank the staff of HRL for preparation of rock and water samples, for the excellent cooperation and the maintenance of our glovebox.

6 References

[Bäc91] Bäckblom, G. 1991. The Äspö hard rock laboratory - a step towards the Swedish final repository for high-level radioactive waste. Tunnelling and Underground Space Technology 4, 463-467.

[Eli1993] Eliason, Th. 1993. Mineralogy, Geochemistry and Petrophysics of Red Coloured Granite Adjacent to Fractures. SKB Stockholm, TR 93-06.

[Fri98] Frieg, B.; Alexander, W. R. ; Dollinger, H.; Bühler, C.; Haag, P.; Möri, A.; Ota, K.; In situ resin impregnation for investigating radionuclide retardation in fractured repository host rocks. Journal of Contaminant Hydrology 35 (1998) 115-130

[Jan98] Jansson, Mats, Erikson, Trygve E. 1998. CHEMLAB In-Situ Diffusion Experiments Using Radioactive Tracers, Radiochimica Acta 82, 153-156.

[Kie2002] KIENZLER, B.; GECKEIS, H.; HAUSER, W.
Actinide Migration in Fractures: Sorption, Redox, Colloids
International TRUE Block Scale Seminar, Oskarshamn, Sweden, Nov 19-20, 2002.

[Kie2002a] KIENZLER, B.; RÖMER, J.; VEJMELKA, P.; JANSSON, M.; ERIKSEN, T.E.; SPAHIU, K. Actinide migration in granite fractures: comparison between in-situ

and laboratory results.
Scientific Basis for Nuclear Waste Management XXVI, Symp.II, MRS Fall Meeting, Boston, Mass., December 2-6, 2002

[Kie2003] KIENZLER, B.; VEJMELKA, P.; RÖMER, J.; FANGHÄNEL, E.; WIKBERG, P.; JANSSON, M.; ERIKSEN, T.E.; Swedish-German actinide migration experiment at ÄSPÖ HRL.
8th Internat.Conf.on Chemistry and Migration Behaviour of Actinides and Fission Products in the Geosphere (Migration '01), Bregenz, A, September 16-21, 2001, Journal of Contaminant Hydrology 61 (2003) 219- 233

[Kie2003a] Bernhard Kienzler, Jürgen Römer, Dieter Schild, Walter Bernotat
Sorption of actinides onto granite and altered material from Äspö HRL
MRS Confernce, Kalmar, June 16-18, 2003

[Kin92] W. Kinzelbach; "Numerische Methoden zur Modellierung des Transports von Schadstoffen im Grundwasser", 2. Auflage, Oldenbourg Verlag, München Wien, 1992

[Rod98] Rodrigues, E.; El Aamrani, F.Z.; Giménez, J.; Casas, I.; Torrero, M.E.; de Pablo, J.; Duro, L.; Hellmuth, K.-H.; Surface characterization of olivine-rock by X-ray photoelectron spectroscopy (XPS). Leaching and U(VI)-sorption experiments, Mat. Res. Soc. Symp. Proc. Vol. 506 (1998) 321-327

[Röm2002] RÖMER, J.; KIENZLER, B.; VEJMELKA, P.; SOBALLA, E.; GÖRTZEN, A.; FUSS, M. Actinide migration experiment in the HRL ÄSPÖ, Sweden: results of laboratory and in situ experiments (Part II). Wissenschaftliche Berichte, FZKA-6770 (Oktober 2002)

[Tul2002] Eva-Lena Tullborg, Terralogica AB, GRÅBO, Descriptions of two samples from drill cores used in the CHEMLAB experiments. Privat communication 2002.

[Vej2000] Vejmelka, P., Fanghänel, Th., Kienzler, B., Korthaus, E., Römer, J., Schüßler, W., Artinger, R., 2000. Sorption and migration of radionuclides in granite (HRL ÄSPÖ, Sweden). Forschungszentrum Karlsruhe, FZKA 6488.

[Vej2001] Vejmelka, P., Kienzler, B., Römer, J., Marquardt, C. M., Soballa, E., Geyer, F., Kisely, T., Heathman, D., 2001. Actinide migration experiment in the HRL ÄSPÖ, Sweden: Results of laboratory and in-situ experiments (Part I). Forschungszentrum Karlsruhe, FZKA 6652.

Appendix A Details from slices of core #5

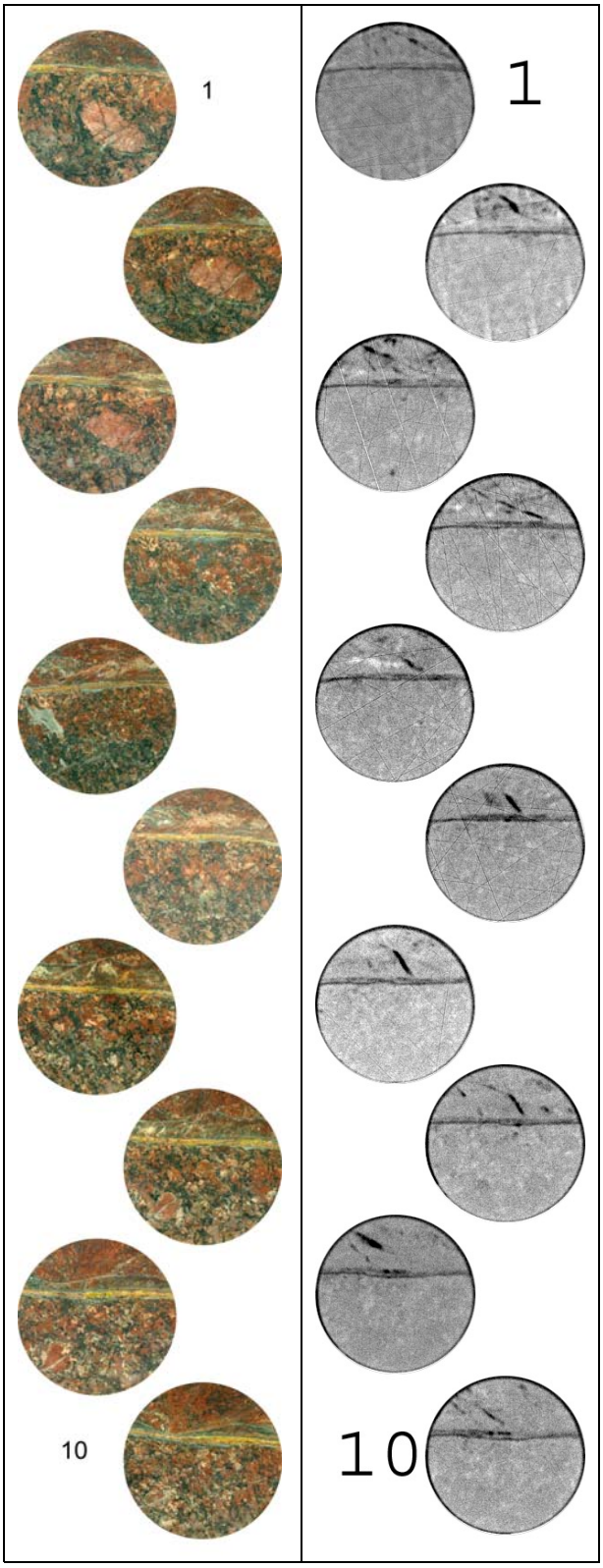

Fig. 6-1 Optical image (left) and corresponding CT image (right) of slices 1 to 10

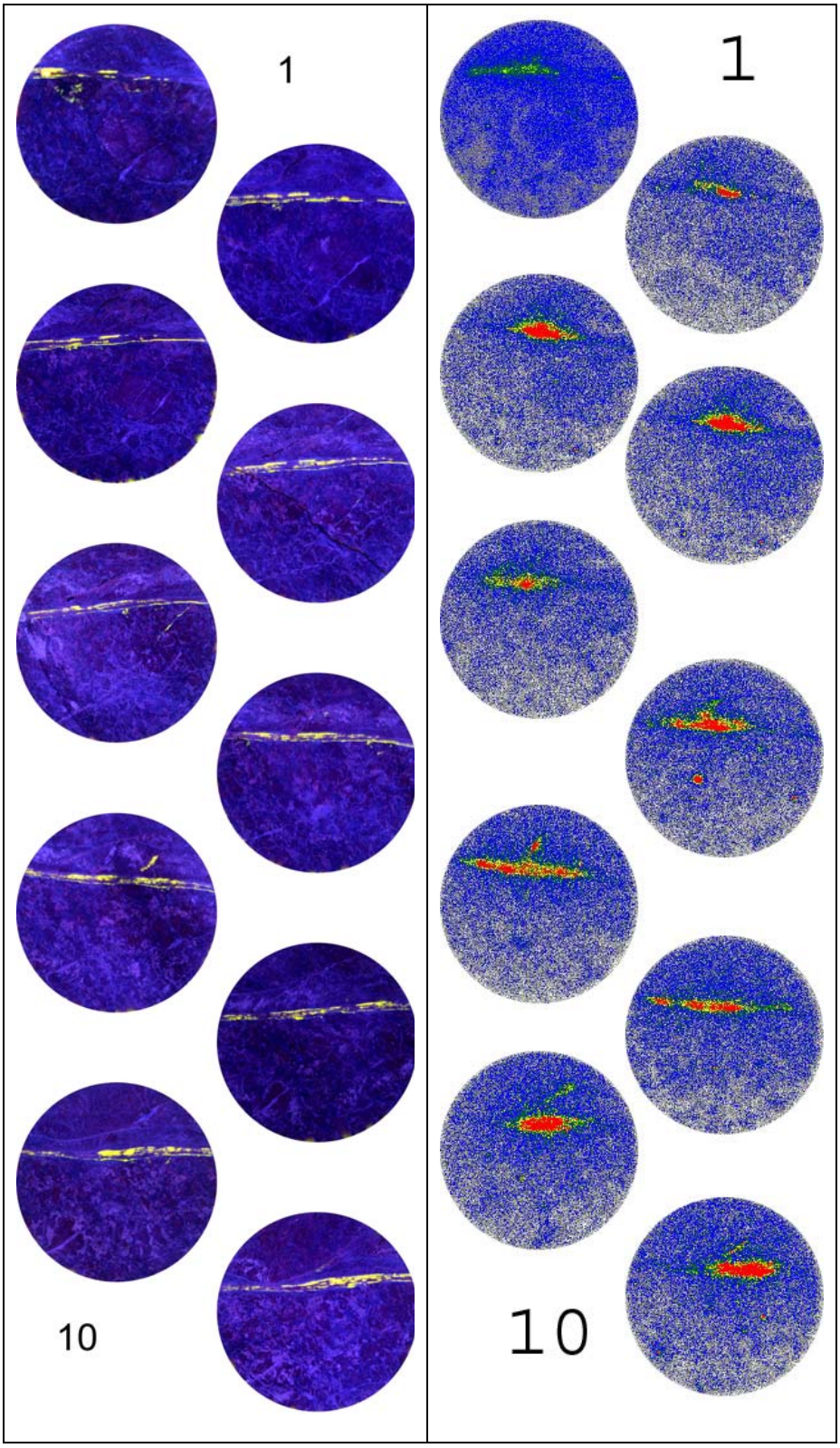

Fig. 6-2 Fluorescence image of the epoxy resin in the fracture (left) and corresponding α-autoradiographic information (right) of slices 1 to 10

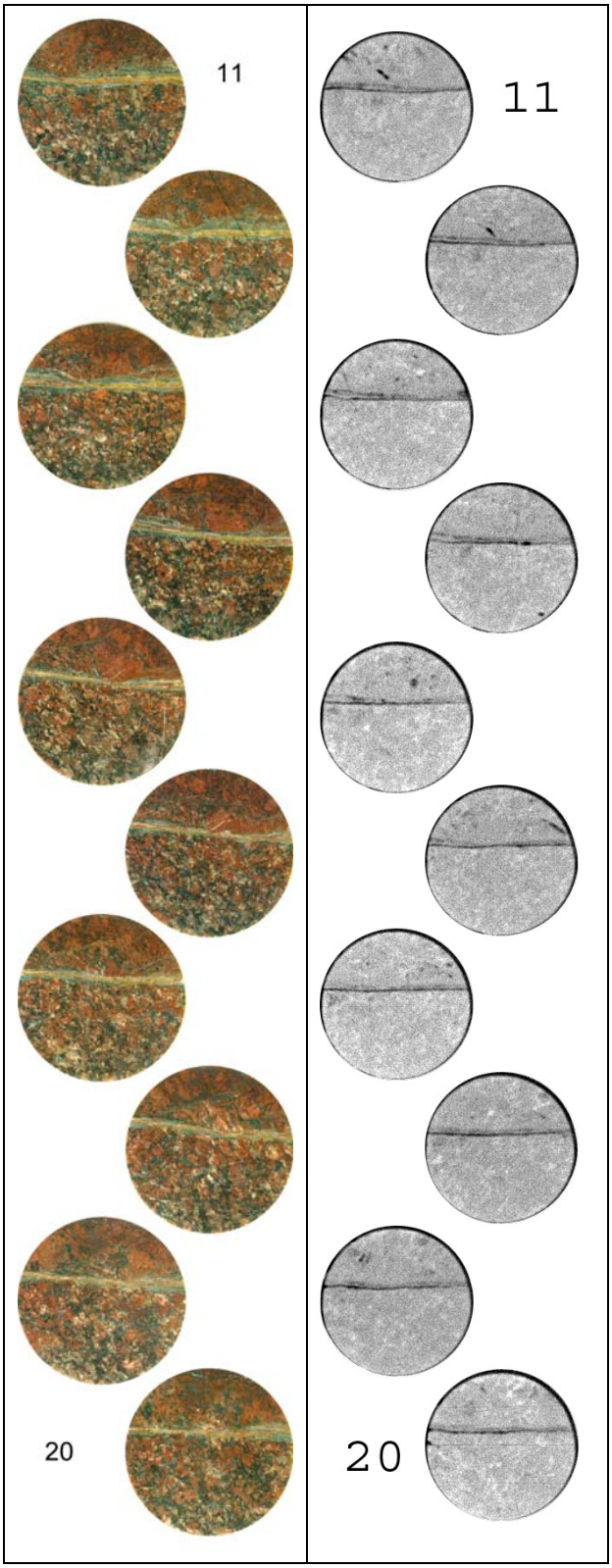

Fig. 6-3 Optical image (left) and corresponding CT image (right) of slices 11 to 20

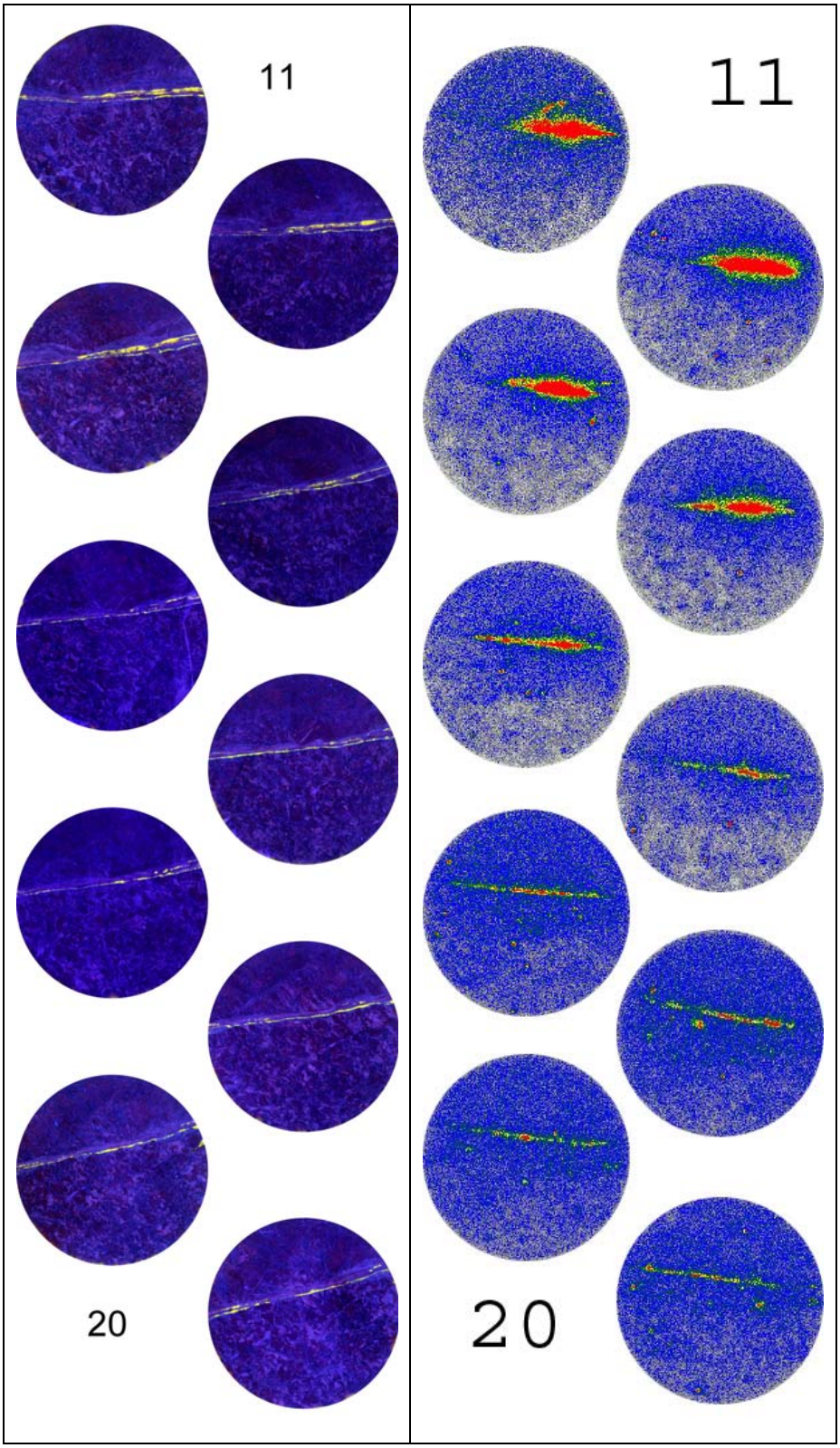

Fig. 6-4 Fluorescence image of the epoxy resin in the fracture (left) and corresponding α-autoradiographic information (right) of slices 11 to 20

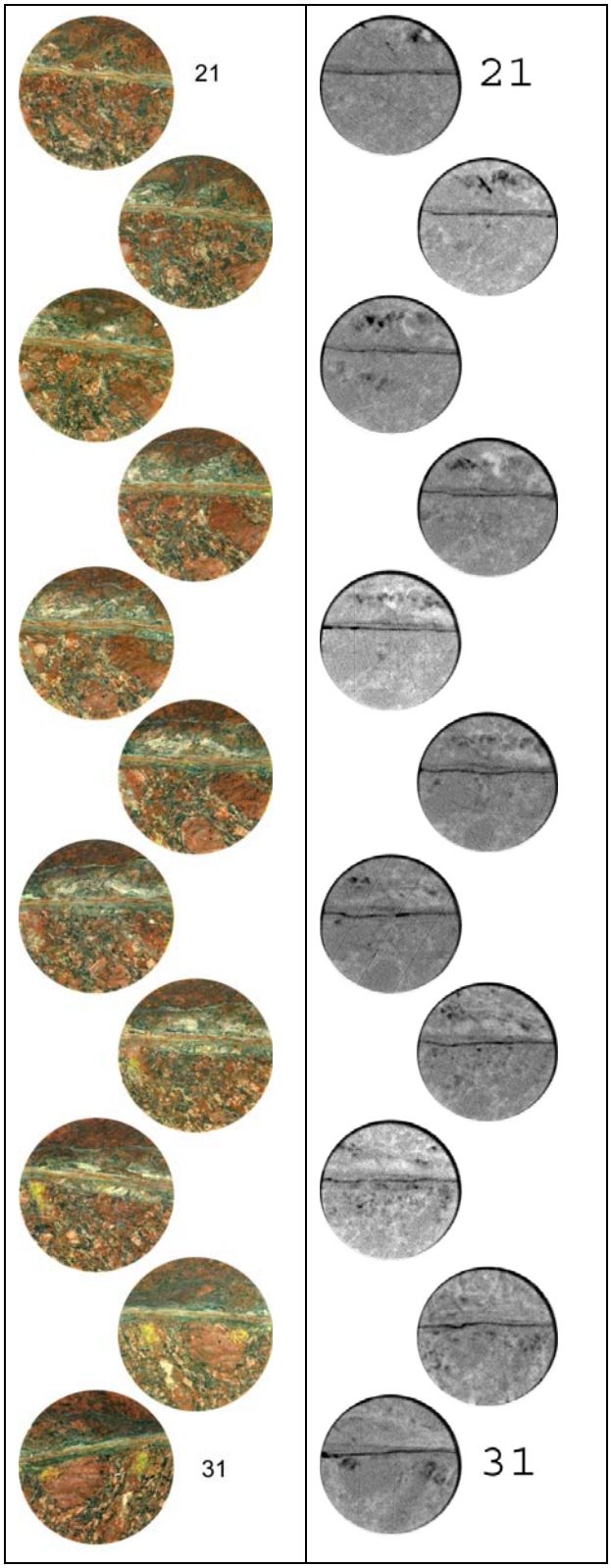

Fig. 6-5 Optical image (left) and corresponding CT image (right) of slices 21 to 31

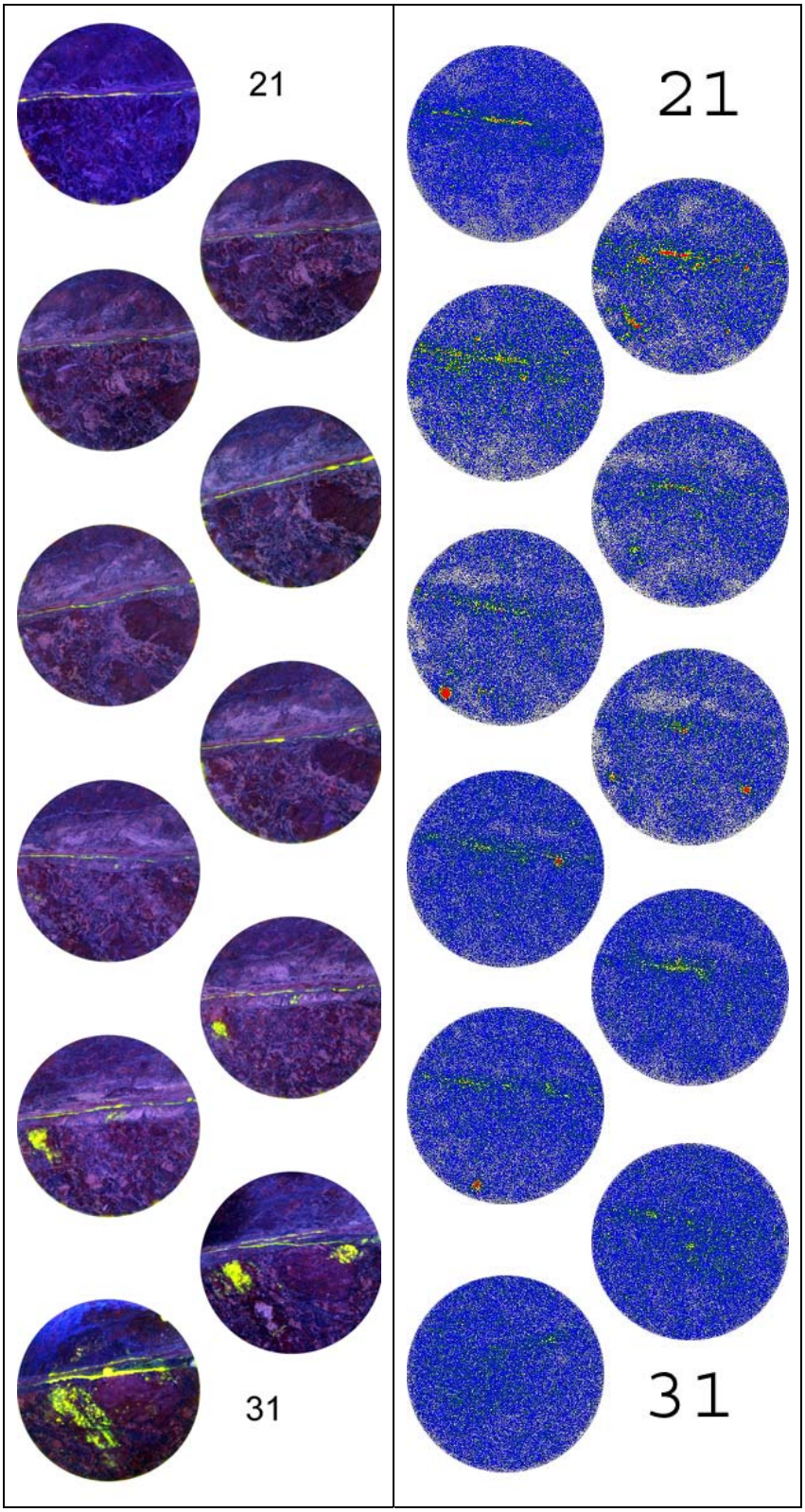

Fig. 6-6 Fluorescence image of the epoxy resin in the fracture (left) and corresponding α-autoradiographic information (right) of slices 21 to 31